https://doi.org/10.5194/gmd-2023-8
Preprint. Discussion started: 17 March 2023

Geoscientific Model Development Discussions

Quantitative Sub-Ice and Marine Tracing of Antarctic Sediment Provenance (TASP v0.1)

James W. Marschalek[1], Edward Gasson[2], Tina van de Flierdt[1], Claus-Dieter Hillenbrand[3], Martin J. Siegert[1,2] and Liam Holder[1]

[1]Department of Earth Science and Engineering & Grantham Institute – Climate Change and the Environment, Imperial College London, Exhibition Road, London, SW7 2BP, UK; j.marschalek18@imperial.ac.uk
[2]Centre for Geography and Environmental Sciences, University of Exeter, Penryn Campus, Cornwall, TR10 9EZ, UK.
[3]British Antarctic Survey, High Cross, Madingley Road, Cambridge, CB3 0ET, UK.

Correspondence to: James W. Marschalek (j.marschalek18@imperial.ac.uk)

Abstract. Ice sheet models must be able to accurately simulate palaeo ice sheets to have confidence in their predictions of future Antarctic ice mass loss and resulting global sea-level rise, particularly over longer timescales. This requires accurate reconstructions of the extent and flow patterns of palaeo ice sheets using real-world data. Such reconstructions can be achieved by tracing the detrital components of offshore sedimentary records back to their source areas on land. However, sediment provenance data and ice sheet model results have not been directly linked, despite the complimentary information each can provide the other. Here, we present a computational framework (Tracing Antarctic Sediment Provenance, TASP) that predicts marine geochemical sediment provenance data using the output of numerical ice sheet modelling. The ice sheet model is used to estimate the spatial pattern of erosion rates and to trace ice flow pathways. Beyond the ice sheet margin, simple approximations of modern detrital particle transport mechanisms using ocean reanalysis data produce a good agreement between our predictions for the modern ice sheet/ocean system and marine surface sediments. Comparing results for the modern system to seafloor surface sediment measurements will allow application of the method to past ice sheet configurations. TASP currently predicts neodymium isotope compositions using the PSUICE3D ice sheet model, but it has been designed so that it could be adapted to predict other provenance indicators or use outputs of other ice sheet models.

https://doi.org/10.5194/gmd-2023-8
Preprint. Discussion started: 17 March 2023

Geoscientific Model Development Discussions

1. Introduction

Antarctic ice flow pathways and ice sheet extent in the geological past can be reconstructed using sediment provenance studies, which trace marine detrital sediments to their constituent source rocks on the continent (e.g. Ehrmann et al., 2011; Cook et al., 2013; Licht and Hemming, 2017; Wilson et al., 2018; Marschalek et al., 2021). However, conclusions about ice sheet extent and flow patterns drawn from such data are typically qualitative. This is because, when viewed in isolation, sediment provenance records can only predict where subglacial erosion was taking place, but often cannot distinguish between changes in ice extent, changes to subglacial conditions which influence erosion rates, or changes to glacimarine sediment transport processes (Wilson et al., 2018; Golledge et al., 2021). Although such complexities are usually considered, interpretations of sediment provenance records are typically limited to a 'nearest-neighbour' type approach, where changes in provenance are attributed to a simple advance/retreat of the ice sheet margin in the vicinity of the core site (e.g. Cook et al., 2013). Numerical modelling offers the potential to make more quantitative estimates of the ice sheet state required to generate observed sediment provenance signatures by predicting the expected provenance of detritus at the ice sheet margin (Aitken and Ursovic, 2021).

Although provenance studies typically focus on past ice sheets, the modern Antarctic ice sheets (i.e. East Antarctic Ice Sheet, West Antarctic Ice Sheet (WAIS) and Antarctic Peninsula Ice Sheet) also offer an excellent opportunity to study how subglacially eroded debris is moved beneath ice. Properties such as surface velocities and ice thicknesses can be directly measured; ice flow drainage pathways are therefore known with a high degree of confidence. These observational data can also be used to invert for parameters such as basal friction coefficients in numerical models, producing predictions of basal stresses (e.g. MacAyeal, 1992; Morlighem et al., 2013). These known variables make estimates of erosion rates and transport pathways of glaciogenic detritus beneath the present-day ice sheets more reliable than those of past ice sheets, despite continuing difficulties predicting processes of erosion and entrainment of subglacial debris (Alley et al., 2019).

Marine processes transporting glaciogenic detritus are another substantial source of uncertainty associated with interpreting glacimarine provenance records which can be more accurately simulated at the present day. The spatial distribution of provenance proxy measurements in marine sediments is far more complete in recent (i.e. late Holocene to modern) surface sediments than in older, more difficult to date, sediments (e.g. Simões Pereira et al., 2018). Here, we make use of these available constraints to calibrate the results of offshore sediment provenance tracing to the observed provenance of seafloor sediments. The approach presented could be adapted for any sediment provenance tracer such as clay minerals (e.g. Ehrmann et al., 2011), heavy minerals (e.g. Hauptvogel and Passchier, 2012), elemental concentrations (Monien et al., 2012), clast petrography data (e.g. Sandroni and Talarico, 2011) or detrital mineral ages (e.g. Licht et al., 2014). We here choose detrital neodymium (Nd) isotopes due to the abundance of available data (e.g. Farmer et al., 2006; van de Flierdt et al., 2007; Roy et al., 2007; Cook et al., 2013; Pierce et al., 2017; Simões Pereira et al., 2018; Marschalek et al., 2021; Robinson et al., 2021). The decay of ^{147}Sm to ^{143}Nd relative to the stable ^{144}Nd isotope gives rocks a $^{143}Nd/^{144}Nd$ signature which is a function of the time since a magma was separated from the mantle and the initial composition of the resulting magmatic rock (Goldstein and Hemming, 2003). This ratio is typically reported in epsilon notation (ε_{Nd}); i.e. in parts per 10,000 compared to the modern Chondritic Uniform Reservoir (CHUR; Jacobsen and Wasserburg, 1980):

https://doi.org/10.5194/gmd-2023-8
Preprint. Discussion started: 17 March 2023

Geoscientific Model Development Discussions

$$\varepsilon_{Nd} = \left(\frac{(^{143}Nd/^{144}Nd)_{sample}}{(^{143}Nd/^{144}Nd)_{CHUR}} - 1\right) \times 10^4 \quad (1)$$

This means rock groups of different lithologies and ages can be differentiated based on their ε_{Nd} value, even if the initial magmatic rock is metamorphosed or eroded. Neodymium isotopes are a powerful sediment provenance proxy as all rock-forming minerals incorporate Nd and Sm into their structure, meaning nearly all rock types will be accounted for and are integrated in the provenance signal. Furthermore, ε_{Nd} is generally unaffected by grain size sorting (Garçon et al., 2013) and the combined provenance signal is expressed simply, as a single number. This makes ε_{Nd} values ideal for tracing in an algorithm tracing sediment provenance.

Geographically, we examine the region offshore of West Antarctica and adjacent areas of East Antarctica (from approximately 60°W to 140°E; Fig. 1). This spans the location of many existing detrital Nd isotope provenance studies (e.g. Cook et al., 2013) and compilations of the ε_{Nd} values of continental rocks (e.g. Simões Pereira et al., 2018; Marschalek et al., 2021). Locations mentioned in the text are displayed in Figure 2.

2. Neodymium Isotope Map

2.1 Approach

To assign eroded detritus an ε_{Nd} value to compare to offshore records, the first requirement is a spatially continuous estimate of ε_{Nd} for the study area below grounded ice (Fig. 1). Constructing this map required the compilation of literature ε_{Nd} data for different rock types. This process was aided by an existing compilation of ε_{Nd} data from the Pacific sector of West Antarctica (Simões Pereira et al., 2018, 2020), extended to the Ross Sea sector (Marschalek et al., 2021). Where the rock sample location was not given in the original publication, coordinates were found by looking up the location name in the SCAR Antarctic Digital Database Map Viewer (https://www.add.scar.org/).

To convert the literature 'point data' into a continuous map, outcropping rocks were grouped. This was facilitated by the recent digital geological mapping of Antarctica from the SCAR GeoMAP project (Cox et al., 2019). To simplify this map, which comprised polygons at a resolution far beyond that required for this study, adjacent outcrops were grouped where subglacial continuity between exposures was deemed reasonable (see example in Fig. 3). For each major rock type, the point ε_{Nd} values were then interpolated and masked to the area of the simplified polygons. A resolution of 10 km was used, which is sufficient given the uncertainties resulting from the ice cover and matches the resolution used in the ice sheet model. These areas of exposed rock can be considered as having a high level of confidence in the final map, particularly when ε_{Nd} values for the outcropping rock group have been measured at numerous localities.

In contrast, most of the study area is covered by ice, making direct geological observations impossible. Pertinent airborne and on-ice geophysical (i.e. gravity, magnetic, subglacial geomorphology obtained by radar) studies were therefore used to inform ε_{Nd} values beneath the ice by making interpretations regarding the subglacial geology (e.g. Jordan et al., 2013a; Goodge and Finn, 2010; Studinger et al., 2006; van Wyck de Vries et al., 2018; Paxman et al., 2019). In some regions, this approach can produce reasonably robust inferences. However, in other areas, relationships between exposed and subglacial geology are more obscure. Even in areas where geophysical constraints are good, the subglacial bedrock there may be hundreds (or thousands) of kilometres

https://doi.org/10.5194/gmd-2023-8
Preprint. Discussion started: 17 March 2023

Geoscientific Model Development Discussions

away from the nearest comparable outcropping rocks. Consequently, using interpolation from the nearest outcrops to assign ε_{Nd} values, as described above for exposed rocks, could lead to bias towards only the geographically nearest measurement. Interpolation may therefore fail to reflect the true variability of the subglacial geology in such areas. To avoid this, areas where a subglacial rock type was predominantly
105 'geophysically'-defined were uniformly assigned a mean ε_{Nd} value based on all suitable measurements of the rock type.

https://doi.org/10.5194/gmd-2023-8
Preprint. Discussion started: 17 March 2023

Geoscientific Model Development
Discussions
Open Access
EGU

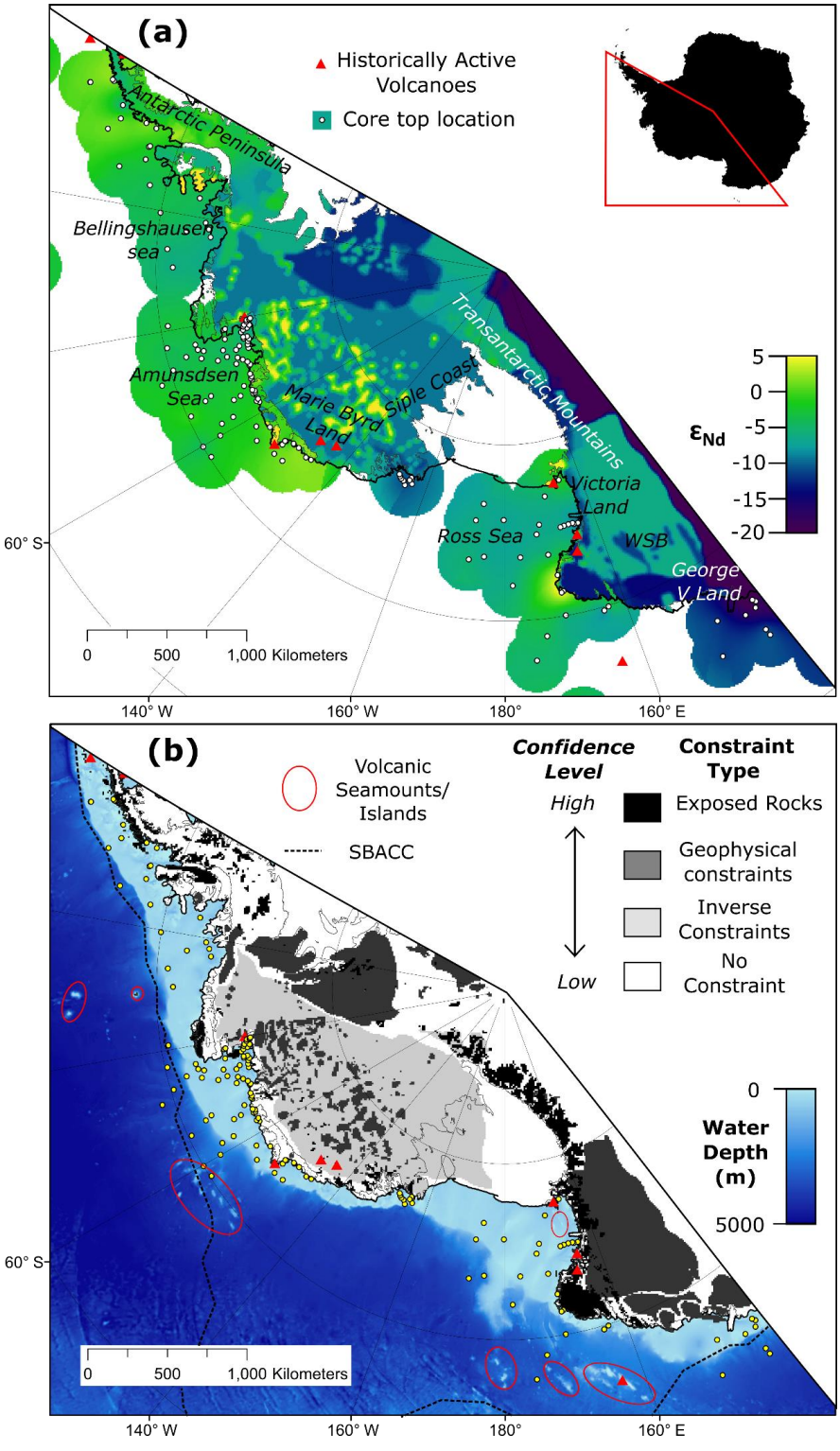

https://doi.org/10.5194/gmd-2023-8
Preprint. Discussion started: 17 March 2023

Geoscientific Model Development Discussions

Figure 1. a) Map of inland ε_{Nd} values used as an input for the provenance tracing and interpolated ε_{Nd} values within 200 km of a marine surface sediment sample with a measured ε_{Nd} value. Seafloor surface sample locations are shown as white circles and volcanoes with reported subaerial eruptions in the historic record are shown in red (Patrick and Smellie, 2013). The MEaSUREs grounding line and modern ice (shelf) fronts are indicated using solid grey and black lines, respectively (Rignot et al., 2013; Mouginot et al., 2017). b) Uncertainty level of ε_{Nd} value estimate, displayed on BedMachine bathymetry (Morlighem et al., 2020). See definitions of the uncertainty levels in the main text. Volcanic seamounts and islands (e.g. Lawver et al., 2012; Kipf et al., 2014) are circled in red. These features are displayed because they potentially supply additional radiogenic detritus to marine sediments which is unaccounted for in our algorithm. The Southern Boundary of the Antarctic Circumpolar Current (SBACC) is shown as a black dashed line (Orsi et al., 1995).

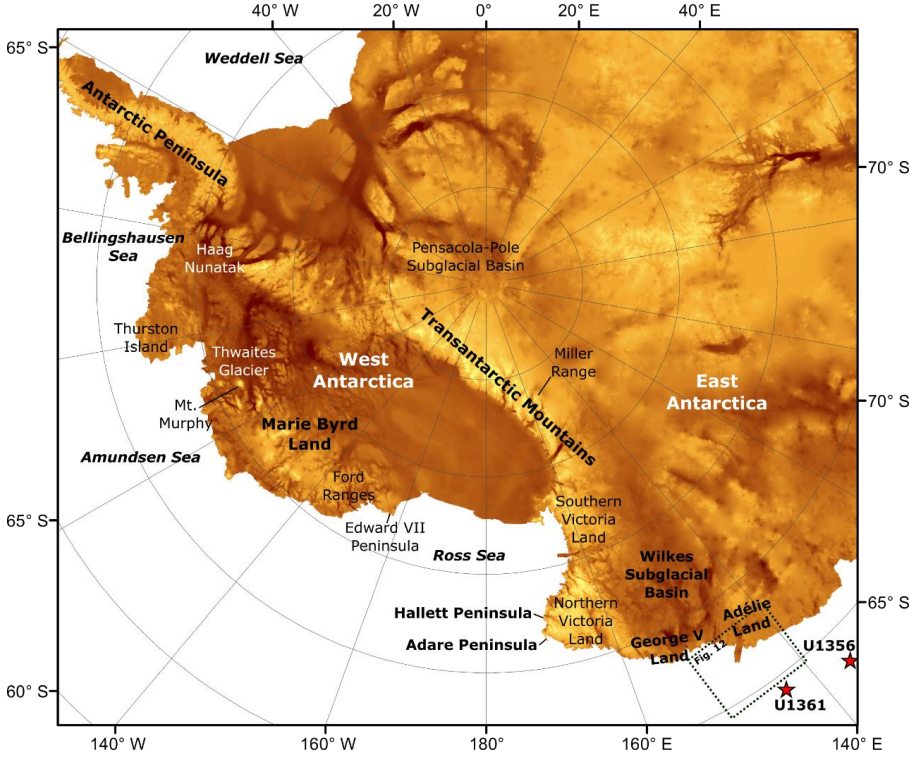

Figure 2. Geographical locations mentioned in the text displayed on BedMachine topography (Morlighem et al., 2020). The area covered by the map shown in Fig. 12 is marked by the box with the black dotted outline.

The sources used to determine the extent of subglacial geology and to estimate the ε_{Nd} value for each rock group are discussed in detail below. To keep the initial offshore ε_{Nd} value estimate as independent as possible, an inverse approach was specifically avoided when constructing the subglacial ε_{Nd} map (i.e. using offshore values to predict onshore ones), except in a few locations where virtually no geophysical or geological data were available as outlined above. A formal inversion for subglacial geochemistry, similar to that recently applied to fluvial provenance (Lipp et al., 2020), would undoubtably provide a much-improved match with modern observations as well as insights into subglacial geology to apply to simulations of past ice sheets. However,

https://doi.org/10.5194/gmd-2023-8
Preprint. Discussion started: 17 March 2023


Geoscientific Model Development Discussions

further development would be required to implement a formal inverse approach in a glacial setting, as additional information beyond an offshore measurement near the ice sheet margin is required to give structure to interior ε_{Nd} values and avoid uniform values along a flow line.

To indicate the approximate uncertainty in the map produced, areas are classified with confidence levels 1-4 (Fig. 1b):

1) Exposed rocks (high confidence; black) – exposed rock with ε_{Nd} data. The quantity and spatial distribution of ε_{Nd} measurements varies between rock types and, in some instances, sparse data meant that the number of data points used in the interpolation across a rock group was low.
2) Geophysical constraints (moderate confidence; dark grey) – areas with subglacial geology constrained by gravimetric/magnetic/geomorphological etc. data. Epsilon Nd values inferred for rock groups are based on the nearest equivalent exposures, but ε_{Nd} values may be different away from the rock outcrop with ε_{Nd} data, or certain rock groups may be over- or under-represented. For instance, in Marie Byrd Land outcrops of Neogene volcanic rocks dominate, but Palaeozoic basement and Cretaceous plutonic rocks are much more widespread (e.g. Rocchi et al., 2006).
3) Inverse/point constraints (low confidence; light grey) – areas with few direct constraints, limited to isolated subglacial samples obtained by drilling through the ice. Epsilon Nd values are determined from these limited samples and surrounding rock exposures, loosely informed by offshore provenance data. This approach differs from a formal inversion as the offshore data are not used to directly predict ε_{Nd} values beneath the ice; instead, they are used to infer what outcropping rock groups are likely to be dominant where there are no other constraints.
4) No estimate made (white) – these are without any rock type constraints, filled using Kriging.

Different rock types have different concentrations of Nd, meaning some rock types will contribute disproportionately to the ε_{Nd} values of subglacial detritus. This effect is not accounted for here due to the uncertainty in concentrations of different rock types, making quantitative assessments challenging. Assuming constant Nd concentration still yields useful results, but the inclusion of variable concentrations in future work would improve the accuracy of our results. Our approach also neglects any pre-glacial sedimentary strata, marine sediments deposited when ice sheets were more retreated than today (e.g. under the WAIS, Wilkes-Adelie Land sectors of the East Antarctic Ice Sheet), or allochthonous subglacial till overlying in-situ bedrock at the base of grounded ice. However, subglacial mixing of detritus is to some degree accounted for by the interpolation of ε_{Nd} values between regions with assigned ε_{Nd} values, as well as assumptions of mean ε_{Nd} values of the surrounding rock types in regions where pre-glacial/marine sedimentary strata or till sheets are likely present under the ice. These simplifications have the effect of smoothing the bedrock ε_{Nd} values. Fully accounting for reworking of subglacial sediments would require a full integration of ε_{Nd} values in time-evolving model runs, which is beyond the scope of this study.

Some regions – particularly the interior of the WAIS towards Marie Byrd Land, the southernmost Transantarctic Mountains and the hinterland of the Bellingshausen Sea – lack even reliable geophysical constraints. In these regions, initial estimates were made by simply interpolating the map produced over the remaining gaps. However, this led to some obvious discrepancies between the ε_{Nd} values of rocks on land and coastal marine sediments. This effect was particularly pronounced in regions of West Antarctica, where geophysical bedrock

https://doi.org/10.5194/gmd-2023-8
Preprint. Discussion started: 17 March 2023

studies typically focus on detecting relatively radiogenic subglacial igneous bodies. The lack of constraint on surrounding rock biases ε_{Nd} values. To account for this, most large areas of the study area with unassigned ε_{Nd} values were prescribed a value informed by sparse subglacial till samples (e.g. Farmer et al., 2006) and surrounding rock types, which markedly improved agreement with marine surface sediment ε_{Nd} values. As spatial variability in ε_{Nd} values is unknown in these regions, the assigned ε_{Nd} values were assumed to be uniform.

2.2 Regional Description of the Neodymium Isotope Map

Here we present a region-by-region summary of the sources used to define the extent and Nd isotope composition of the bedrock of West Antarctica and adjacent areas of East Antarctica. A description of geological formations, lithologies and the tectonic framework of the study area is not relevant to this study and so is not discussed here. For recent reviews of East Antarctic, West Antarctic and Transantarctic Mountain geology, see Boger (2011), Jordan et al. (2020a) and Goodge (2020), respectively.

2.2.1 George V Land and the Wilkes Subglacial Basin

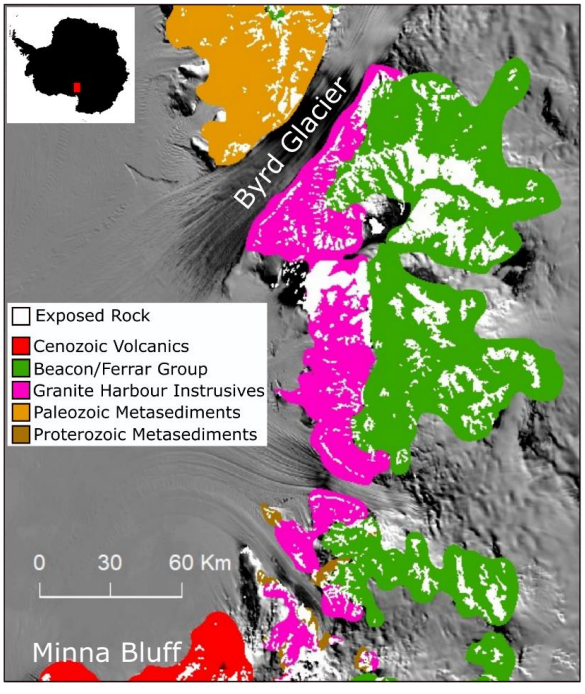

Figure 3. Example of the high-resolution rock polygons from GeoMAP (white; Cox et al., 2019) versus the simplified polygons used to construct the ε_{Nd} value map (coloured). The latter are sufficient at the >~10 km resolution of interest here. The region shown is a section of the Transantarctic Mountains between Byrd Glacier and Minna Bluff. The geology is overlain on MODIS imagery (Haran et al., 2014). The location within Antarctica is indicated in the upper left inset.

https://doi.org/10.5194/gmd-2023-8
Preprint. Discussion started: 17 March 2023

The extent of pre-Cambrian East Antarctic rocks is mapped according to Goodge and Finn (2010), which is broadly consistent with ADMAP2 magnetic anomalies (Golynsky et al., 2018). The coastal extent of these pre-Cambrian rocks is based on interpretation of these data in Bertram et al. (2018). Limited measurements of this rock group give spatially variable ε_{Nd} values, spanning approximately -33 to -11 in the Miller Range of the central Transantarctic Mountains (Borg et al., 1990; Borg and DePaulo, 1994), -24 to -22 along the Adélie Land coast (Peucat et al., 1999), and -16 to -15 at the bed of the EPICA Dome C ice core (Delmonte et al., 2004). The pre-Cambrian rocks are assigned a uniform ε_{Nd} value of -20, which is considered reasonable given the limited exposure of these rocks. Beyond the edge of the area studied, no attempt was made to compile literature ε_{Nd} values as erosion rates are low (e.g. Jamieson et al., 2010) and the Antarctic Coastal Current will carry any detritus reaching the coast westwards out of the study area (e.g. Fig. 6). Rocks in other parts of Antarctica are thus unlikely to substantially impact the provenance signature of the regions studied offshore here, although some ice flowlines do cross beyond the study area shown in Fig. 1. Based on the assumptions described above, the rest of East Antarctica was also assigned a uniform ε_{Nd} value of -20.

Exposures of the late Neoproterozoic to Ordovician Wilson, Bowers and Robertson Bay Terranes are widespread throughout Northern Victoria Land. For these three respective rock groups, measured ε_{Nd} values range from -22.6 to -11.1 (Talarico et al., 1995; Henjes-Kunst and Schussler, 2003; Estrada et al., 2016), -19.9 to -10.5 (Tonarini and Rocchi, 1994; Henjes-Kunst and Schussler, 2003) and -15.6 to -12.3 (Henjes-Kunst and Schussler, 2003). However, most measurements cluster around a mean ε_{Nd} value of approximately -14, which is assigned uniformly to these groups.

Granite Harbour Intrusive rocks are exposed in Victoria Land and, although these have relatively uniform ε_{Nd} values with a mean of ~-12 (Cox et al., 2000; Armienti et al., 1990; Dallai et al., 2003; Rocchi et al., 1998; 2009), their ε_{Nd} values are allowed to vary spatially in our ε_{Nd} map. These granitic rocks are also suggested to be present in the Wilkes Subglacial Basin, but the southern and northern extent and depth of these subglacial granitic bodies are subject to significant uncertainty (Ferraccioli et al., 2009).

The youngest rocks in the Wilkes Subglacial Basin are Ferrar Group dolerites and basalts, which intrude and overlay Beacon Supergroup siliciclastic rocks. The extent of these rock types beyond their very limited outcrops is estimated using the previous interpretation of geophysical data in Bertram et al. (2018), with more southern limits mapped according to Jordan et al. (2013a). Jordan et al. (2013a) show a greater extent of Beacon/Ferrar Group rocks compared to the interpretations of Studinger et al. (2006) in Southern Victoria Land; we favour this more recent interpretation. Ferrar Group dolerites and basalts are isotopically well-constrained and consistent, with mean ε_{Nd} values of ~-6 (e.g. Elliot et al., 1999; Hergt et al., 1989; Molzahn et al., 1996). The ε_{Nd} values in Beacon Supergroup rocks are much more varied and sparsely measured, with mean values around -12 (Fleming, 1995; Bertram, 2018; Marschalek et al., 2021). Given that (i) the relative abundance of these rocks is uncertain but Ferrar sills are common through the Wilkes Subglacial Basin (Ferraccioli et al., 2009), (ii) concentrations of Nd are approximately twice as high in Ferrar Group rocks than Beacon Supergroup rocks (Bertram, 2018), and (iii) the uppermost Beacon Supergroup rocks have a Ferrar-like isotopic composition (Elliot et al., 2017), we assume an ε_{Nd} value of -7 is reasonable for a typical mixture detritus originating from Beacon and Ferrar Group rocks.

https://doi.org/10.5194/gmd-2023-8
Preprint. Discussion started: 17 March 2023


Geoscientific Model Development Discussions

Areas between the coast and Beacon/Ferrar Group rocks are assumed to be a mixture of Lower Palaeozoic rocks (i.e. Wilson Group, Bowers Group, Granite Harbour Intrusive and Robertson Bay Terranes), which are known to be present subglacially based on Miocene sediments recovered at from Integrated Ocean Drilling Program (IODP) Expedition 318 Site U1359 (Pandey et al., 2018). Based on the most unradiogenic ε_{Nd} values measured in nearby seafloor surface sediments (~-15.5; Cook et al., 2013), this local endmember may be slightly more unradiogenic than the -14 to -12 described above; we therefore opt for an ε_{Nd} value of -15 here. Sedimentary basins in the Wilkes Subglacial Basin (Frederick et al., 2016) are ignored, as it is assumed these would be comprised of mixtures of relatively local bedrock and are therefore accounted for using mean ε_{Nd} values for each rock type.

2.2.2 Southern Victoria Land and Transantarctic Mountains

The central Transantarctic Mountains provide some of the most extensive rock outcrops in Antarctica (Goodge, 2020). Neodymium isotope composition measurements are also plentiful for many rock types, making this a well-constrained region. We use the mapping of Cox et al. (2019) and isotopic data compiled and referenced in Marschalek et al. (2021) to produce the ε_{Nd} value map here. In the Transantarctic Mountains, there are outcrops of the pre-Cambrian and Beacon Supergroup/Ferrar Group rocks discussed above. Other rock types with ε_{Nd} measurements include the Neoproterozoic to early Paleozoic metasedimentary Skelton, Byrd, Beardmore and Liv groups (e.g. Borg et al., 1990; Borg and DePaulo, 1994; Cox et al., 2000; Goodge et al., 2008) and Palaeozoic Granite Harbour Intrusives (e.g. Goodge et al., 2012; Borg et al., 1990; Borg and DePaulo, 1994; Cox et al., 2000).

On the East Antarctic side of the southern Transantarctic Mountains, we extend the Ferrar Group and Beacon Supergroup into the Pensacola-Pole subglacial basin based on interpretations by Paxman et al. (2019). The Precambrian East Antarctic craton, the extent of which is defined by Goodge and Finn (2010), is prescribed an ε_{Nd} value of -20 as described above. In the area between rock exposures in the southern Transantarctic Mountains and geophysical data around the South Pole, relatively little is known about the subglacial geology due to a lack of data; thus, the gap was initially simply interpolated across. However, predicted ε_{Nd} values at the ice sheet margin for this portion of the Transantarctic Mountains were consistently too radiogenic (~-5) compared to recent ε_{Nd} values beneath Whillans Ice Stream (~-8 to -9) and in the Ross Sea (~-7 to -8) (Farmer et al., 2006; Marschalek et al., 2021). This may be due to a bias towards exposures of the Granite Harbour Intrusive rocks, which have a mean ε_{Nd} value of -4.6 (n = 10) in this region (Borg et al., 1990; Borg and DePaulo, 1994). These rocks are likely to be more resistant to erosion than the surrounding sedimentary rocks such as those of the Liv Group and Beacon Supergroup, meaning they may outcrop a disproportionate amount. There may also be bias towards exposure or measurement of more radiogenic beds in the Liv Group (e.g. Wareham et al., 2001).

To combat this bias, we assigned a uniform ε_{Nd} value of -9 around rock outcrops, based on the limited measurements of Beardmore and Liv Group metasediments, which likely comprise the bedrock between the Granite Harbour Intrusive batholiths (Marschalek et al., 2021). An ε_{Nd} value of -9 is also comparable to two measurements of the Beacon Supergroup in the southern Transantarctic Mountains (Marschalek et al., 2021).

https://doi.org/10.5194/gmd-2023-8
Preprint. Discussion started: 17 March 2023

Geoscientific Model Development Discussions

To the north, the youngest rocks in this region belong to the Cenozoic McMurdo Volcanic Group in Victoria Land. These are heavily sampled and allowed to vary spatially in our map, but are generally consistent with a mean ε_{Nd} value of +5.3 ± 0.6 (e.g. Avaido et al., 2015; Martin et al., 2013; Phillips et al., 2018).

2.2.3 Siple Coast and central West Antarctica

Ice cover is extensive and geophysical data are limited in the West Antarctic interior, making it difficult to constrain the sub-ice geology there. However, till samples from beneath ice streams and in the Ross Sea provide some guidance to the likely subglacial lithologies (Farmer et al., 2006; Licht et al., 2014). Underlying much of this region are subglacial sedimentary basins, which range in age from the opening of the West Antarctic rift system in the mid-Cretaceous through to the Pliocene or Pleistocene (LeMasurier and Landis, 1996). Studies of sediment provenance suggest which rocks may be contributing (Farmer et al., 2006; Licht et al., 2014; Marschalek et al., 2021), including:

- A late plutonic phase of the Ross orogeny towards the Transantarctic Mountains (i.e. Granite Harbour Intrusives, see references above);
- Cretaceous to Triassic granitic rocks (e.g. Weaver et al., 1992; Craddock et al., 2017; Pankhurst et al., 1998);
- Palaeozoic (meta-)sedimentary rocks such as the Swanson Formation in western Marie Byrd Land and equivalents in the Whitmore Mountains (e.g. Korhonen et al., 2010; Yakymchuk et al., 2015); and
- Palaeozoic granitic rocks such as the Ford Granodiorite in westernmost Marie Byrd Land (e.g. Weaver et al., 1992; Yakymchuk et al., 2015; Korhonen et al., 2010).

Potential mixture of these lithologies in the sedimentary bed based on adjacent exposed rocks suggests an ε_{Nd} value of ~-10 (Table 1). This value agrees well with that of the most unradiogenic sediments beneath the Siple Coast ice streams (Bindschadler Ice Stream), so is thought to be representative (Farmer et al., 2006). A uniform ε_{Nd} value of -10 was therefore assigned to the entire West Antarctic interior. The magnitude and extent of contribution from Granite Harbour Intrusive rocks is difficult to constrain, but as these rocks have a mean ε_{Nd} value of ~-10 (Borg et al., 1990; Borg and DePaulo, 1994; Goodge et al., 2012), they may not influence the overall composition very much, so they are neglected (Table 1).

Table 1. Endmember assignment for central West Antarctica. The term "West Antarctic sediments" refers to our approximation for all sediments likely to underlie the WAIS since the opening of the West Antarctic rift system, including pre-glacial sediments, marine sediments deposited during ice-free periods, and subglacial till. It is assumed the surrounding rock types forming the source rocks for these sediment types has probably remained the same throughout the Cenozoic.

Rock Group	Mean [Nd]	Fraction	Mean ε_{Nd}
Palaeozoic (meta)sedimentary rocks	41	0.55	-11.3
Palaeozoic Granitoids	29	0.225	-6.8
Mesozoic Granitoids	12	0.225	-7.0
Mixture (West Antarctic sediments)	32	-	**-10.0**

https://doi.org/10.5194/gmd-2023-8
Preprint. Discussion started: 17 March 2023


Geoscientific Model Development Discussions

It is generally agreed that some Cenozoic volcanic rocks also exist beneath the WAIS. The locations for these Cenozoic volcanic rocks were initially set based on exposed volcanoes, the subglacial volcano inventory of van Wyk de Vries et al. (2017) and the survey of Lundyk (2003). Preliminary application of the algorithm also found their presence is required to explain sufficiently radiogenic ε_{Nd} values offshore, assuming surrounding rocks have values of -10 as described above. The extent of these volcanic rocks is subject to some uncertainty (Andrews and LeMasurier, 2021) and volcanic rocks comprise only a small fraction of gravel-sized detritus in the eastern Ross Sea, but it is possible these rocks have been crushed to finer grain sizes by a combination of physical weathering and glacial comminution (Perotti et al., 2017).

Even when these potential volcanic rocks were included, ε_{Nd} values were not radiogenic enough to match offshore provenance observations. This may be linked to the uniform ε_{Nd} value of -10 applied for West Antarctic sediment. More radiogenic granitic rocks, potentially similar to the most radiogenic granitoids in the Ford Ranges (Korhonen et al., 2010) or on Thurston Island (Pankhurst et al., 1993), may be widespread in some areas beneath the WAIS, as unexposed Mesozoic-aged rocks are clearly present based on detrital zircon ages (Licht et al., 2014; Marschalek et al., 2021). However, without data to constrain the extent and isotopic composition of these rocks, we favour the addition of extra Cenozoic volcanic rocks to improve the match with observations. Behrendt (2013) correlated magnetic anomalies in the WAIS interior to subglacial late Cenozoic volcanic rocks. We assume that such rocks occur at sites with high magnetic anomalies based on the ADMAP-2 compilation (Golynski et al., 2018). Although this is a crude approach, new detailed mapping of possible volcanic material or more radiogenic granitic rocks beneath the WAIS is beyond the scope of this study. Indeed, understanding the mixture of rocks beneath the central WAIS would be greatly beneficial for future sediment provenance studies seeking to study WAIS collapse.

A uniform ε_{Nd} value of +5.3 was selected for Cenozoic volcanic rocks based on the consistent isotopic signature of such rocks throughout Marie Byrd Land and Victoria Land (Avaido et al., 2015; Martin et al., 2013; Phillips et al., 2018; Futa and LeMasurier, 1983; Hart et al., 1995). We emphasise, however, that the Kriging interpolation and 10 km spatial resolution used in our map implies that small areas of volcanic material will not result in such a high value. This was an intentional effect to partially account for the uncertainty in the presence of these subglacial volcanic rocks.

Adjacent to the Edward VII Peninsula, where outcropping rocks are sparse, the model consistently predicted ε_{Nd} values that were too radiogenic in comparison with seafloor surface sediment values which reach a mean of -11.1 ± 0.4 (n = 8) (Simões Pereira et al., 2018; Carlson et al., 2021). This was likely a result of an underrepresentation of the Swanson Formation on the Edward VII Peninsula in western Marie Byrd Land, as this rock group shows a close geochemical affinity with the glacimarine shelf sediments in this area and may be widespread beneath the WAIS here (Simões Pereira et al., 2018). It was therefore assumed that the Swanson Formation, with an ε_{Nd} value of ~-12 (Korhonen et al., 2010; Yakymchuk et al., 2015), lies beneath most of the ice on the Edward VII Peninsula.

2.2.4 Amundsen and Bellingshausen Sea drainage sectors

Rock exposures around the Amundsen Sea embayment are particularly limited. Granites inferred to be present are assumed to be extensions of Mesozoic outcrops along this coast. Cenozoic volcanics are extended, largely

https://doi.org/10.5194/gmd-2023-8
Preprint. Discussion started: 17 March 2023

under Thwaites Glacier, using interpretations of magnetic, gravimetric, and topographic data (Jordan et al., 2020b) as well as airborne radar data that indicate enhanced subglacial melting due to elevated geothermal heat flux (Schroeder et al., 2014). Mafic rocks are assumed to include gabbros of Cenozoic age (Simões Pereira et al., 2020), similar to Dorrell Rock near Mt. Murphy. The bedrock surrounding these intrusions is assumed to be a mixture of typical West Antarctic rocks and assigned an ε_{Nd} value of -10 as described above.

A lack of rock outcrops and geophysical data translate to large uncertainties in the Bellingshausen Sea drainage sector of the WAIS (Fig. 1b). The Mesozoic granites and Antarctic Peninsular Volcanic Group present in the Antarctic Peninsula region, including the coastal region of the eastern Bellingshausen Sea, are extended based on continuation of magnetic anomalies, but there are no outcrops to confirm this assumption is correct. Values are predominantly set to -10 as described above for the WAIS interior, assuming a similar mixture of rock types present. This matches with the ε_{Nd} values of sediments from beneath the floating terminus of Pine Island Glacier, which drains part of this region into the SE Amundsen Sea embayment (Simões Pereira et al., 2020).

2.2.5 Antarctic Peninsula

Rocks are relatively well exposed along the Antarctic Peninsula, with lithological extrapolation between outcrops possible using geophysical data (Golynski et al., 2018) and geological mapping (Burton-Johnson and Riley, 2015). The ε_{Nd} values of many rock types are, however, relatively poorly constrained (see references in Simões Pereira et al., 2018 for available measured rock ε_{Nd} values). Fortunately, there is relatively little variation in Nd isotope compositions in this geologically young region, with ε_{Nd} values commonly ranging from ~-6 to -2, although some rocks have ε_{Nd} values clustered around ~-10 to -8 and ~+1 to +3 (Simões Pereira et al., 2018 and references therein). However, a relative lack of variation means uncertainty here is unlikely to substantially influence our results.

2.2.6 Western Weddell Sea (West Antarctic side)

The extent of the Haag nunatak block is taken from Jordan et al. (2020a). It is possible this is overlain or intruded by rock types representing a continuation of Jurassic volcanic/magmatic activity recorded in rock outcrops on the Antarctic Peninsula. Furthermore, provenance data suggest that old (meta)sediments may be present on top of the Haag nunatak block as the mean ε_{Nd} value of ~-7.4 for these rocks (Storey et al., 1994) is more radiogenic than that for seabed sediments recovered offshore from this part of the Ronne Ice Shelf (Williams et al., 2017).

Most rocks around the western Weddell Sea embayment are Cambrian-Permian sedimentary rocks, Cambrian volcanics or Mesozoic granites. Exposures are extended based on Jordan et al. (2013b), assuming outcrops are broadly representative of rocks present beneath the ice. The Cambrian volcanics and Mesozoic granites have been isotopically characterised, with respective mean ε_{Nd} values (±2SD) of -3.5±4.3 (Curtis et al., 1999) and -6.6±3.4 (Pankhurst et al., 1991; Borg and DePaulo, 1994; Craddock et al., 2017), but no known ε_{Nd} measurements of the widespread Cambrian-Permian sedimentary strata have been performed. An ε_{Nd} value of -13 is assumed to be representative of these rocks, based on temporal equivalents in the southern Transantarctic Mountains, such as the Byrd Group and non-volcanic beds of the Liv Group (Borg et al., 1990; Goodge et al., 2008; Marschalek et al., 2021). Neodymium isotope compositions of offshore sediments agree with this

https://doi.org/10.5194/gmd-2023-8
Preprint. Discussion started: 17 March 2023

Geoscientific Model Development Discussions

hypothesis (Williams et al., 2017). Beacon Supergroup and Ferrar Group outcrops in the Weddell Sea drainage sector follow the published mapping by Paxman et al. (2019) (see Transantarctic Mountain section). The extent of the Dufek intrusion (part of the Ferrar Group) is based on Ferris et al. (1998). Although we include the Weddell Sea drainage sector of the WAIS in our mapping, we do not include predictions for Weddell Sea offshore sediments in our results as these will also be influenced by supply of glaciogenic debris from East Antarctica; i.e., from sources which are outside of our compilation area.

2.3 Data from Recent Seafloor Surface Sediments

To assess the accuracy of our sediment provenance tracing, comparison to measurements of ε_{Nd} in recent seabed surface sediments was conducted. These data were compiled from all known literature sources in our study domain (Walter et al., 2000; Roy et al., 2007; van de Flierdt et al., 2007; Pierce et al., 2011; Cook et al., 2013; Struve et al., 2017; Simões Pereira et al., 2018, 2020; Carlson et al., 2021; Shao et al., 2022). New seafloor surface sediment ε_{Nd} data from the Ross Sea were also included to improve spatial coverage in this area (Table 2).

Table 2. Neodymium isotope data for new surface sediment samples in the Ross Sea.

Site	Sample depth	Latitude	Longitude	Water depth (m)	$^{143}Nd/^{144}Nd$	ε_{Nd}	± 2σ S.E.	± 2 S.D.
G837	Surface grab	-67.70	175.33	3430	0.512341	-5.80	0.000010	0.29
Procedural replicate					0.512358	-5.47	0.000011	0.27
Procedural replicate					0.512363	-5.37	0.000010	0.27
Procedural replicate					0.512339	-5.84	0.000010	0.29
A524	Surface grab	-73.33	187.20	3566	0.512336	-5.90	0.000008	0.29
A461	Surface grab	-73.53	171.37	564	0.512326	-6.08	0.000011	0.29
A452	Surface grab	-75.58	186.70	1253	0.512283	-6.92	0.000010	0.29
A523	Surface grab	-73.57	184.22	2762	0.512252	-7.53	0.000009	0.29
E194	Surface grab	-71.30	170.00	106	0.512921	5.51	0.000010	0.29
E196	Surface grab	-71.37	169.67	320	0.512864	4.41	0.000010	0.29
E183	Surface grab	-72.31	170.19	146	0.512855	4.23	0.000009	0.29
IODP U1521	4-6 cm	-75.68	-179.67	562	0.512243	-7.70	0.000009	0.26
IODP U1522	2-5 cm	-76.55	-174.76	558	0.512252	-7.53	0.000006	0.29

The methods used to generate these new data are identical to those described in Simões Pereira et al. (2018) and Marschalek et al. (2021). Briefly, the <63 µm fractions were leached to remove authigenic coatings, digested and subject to standard ion exchange chromatography to isolate the Nd. The $^{143}Nd/^{144}Nd$ ratio was measured on a Nu instruments HR-ICP-MS in the MAGIC laboratories at Imperial College London. Measurements of BCR-2 processed alongside samples were consistently within error of the published value (Weis et al., 2006) and blanks were 13 pg.

https://doi.org/10.5194/gmd-2023-8
Preprint. Discussion started: 17 March 2023

Geoscientific Model Development Discussions

3. Debris Generation and Subglacial Transport

3.1 Ice Sheet Model and Erosion Rate

TASP is separate from the ice sheet model and can therefore be applied to the results of other ice sheet models providing key outputs (basal velocities, basal shear stress and ice thickness) are saved.

The results presented here all use the ice sheet model PSUICE3D, which uses a finite-difference numerical model with hybrid ice flow dynamics (Pollard and DeConto, 2012). Following the approach of Pollard and DeConto (2019), erosion rate (E) is calculated as proportional to the product of basal velocity (u_b) and basal shear stress (τ_b):

$$E = \tau_b u_b k \quad (2)$$

The 'quarrying' coefficient k is a parameter dependant on properties including the erodibility of different rock types and other parameters which are unaccounted for. Here, a constant value of 5.1 x 10^{-10} was used for k as suggested by Pollard and DeConto (2019). As we are concerned only with relative, and not absolute, quantities of detritus the value used will not impact results. Experiments were also performed with spatially variable k values for different sectors of Antarctica tuned to the quantity of marine sediment deposited on the Antarctic continental margin since 40 Ma (Pollard and DeConto, 2019). However, this yielded a negligible change to the match with seafloor surface sediment ε_{Nd} values than using a constant k.

The approach presented here differs from the method used to predict offshore sediment provenance from numerical modelling by Aitken and Urosevic (2021), who used the squared basal velocity (capped at 600 m/yr) as an erosion rate proxy. Furthermore, these authors used a 20 km resolution instead of our 10 km resolution, as well as a Bayesian inference approach accounting for uncertain geological variation. However, the primary distinction between our approach and this previous study is our inclusion of detritus transport in the marine realm, discussed in Sect. 4.

3.2 Tracing the Generation and Subglacial Transport of Detritus

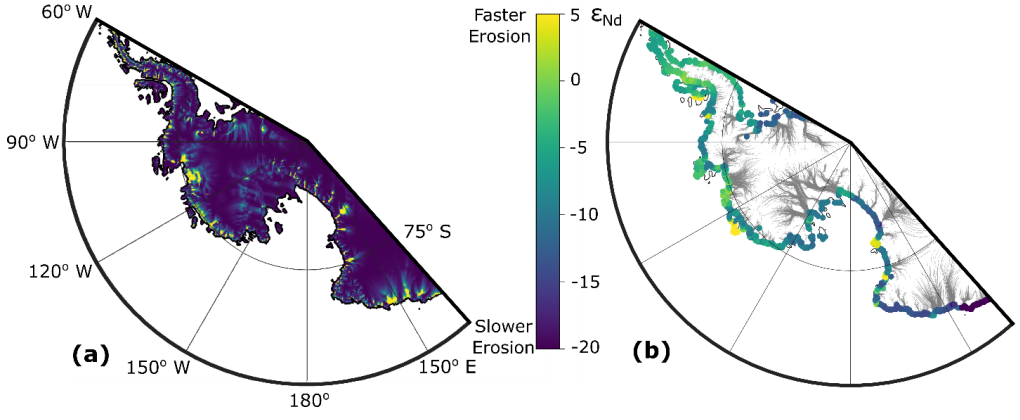

https://doi.org/10.5194/gmd-2023-8
Preprint. Discussion started: 17 March 2023

Figure 4. a) Erosion rate map used to seed start locations. Absolute erosion rates are not given as these are uncertain and not required to predict offshore provenance. b) An example of grounded ice flow lines (grey) generated by random sampling using 16000 seed locations, with points at the end of each flow line coloured according to the ε_{Nd} value at the flow line start point. The colour bar in the centre shows both the erosion rate in panel a) and the ε_{Nd} values in panel b).

The provenance of the detritus reaching the ice sheet margin was modelled using the ice sheet model erosion rate. This was performed using two different methods:

1) **Random generation of seed locations for flowlines based on the erosion rate.** Here, seed locations in the grounded portion of the ice sheet model grid were selected based on the erosion rate at the given location, with a given point proportionally more likely to be selected if the erosion rate was higher (Fig. 4). This was performed by totalling the erosion rate value of all cells and calculating the fraction each cell represents of this total, then generating a random number and selecting a cell based on this probability. A cell could be selected multiple times. Following this, the flow path the detritus at each seed location took to the ice sheet margin was traced using the 'streamline' function in MATLAB. Using the basal velocity ice sheet model output, this traced the flow paths of ice, and thus glacigenic detritus, to the ice sheet margin (Fig. 4b). The end point location was assigned the ε_{Nd} value of the source location and then, once all streamlines were calculated, each cell at the ice sheet margin was set to the mean value of all the streamlines terminating in it. To minimise the effects of random sampling, 32,000 seed locations were typically generated, which was considered a suitable compromise between computational time and accuracy (Fig. 5). When using this method, the default MATLAB random number stream was always reset to remove any (minor) effects of random sampling.
2) **Calculation of all flowlines weighted based on erosion rate.** Following this method, seed locations were selected based on a user-defined erosion rate threshold which by default was set to 0 to include all cells beneath grounded ice. Sediment packages were traced to the ice sheet margin as described for the random generation method. However, the ε_{Nd} value at the ice sheet margin was instead set by weighting flowlines proportionally based on the erosion rate rather than using just a mean. An advantage compared to the random generation method is the lack of random variability and avoiding multiple selections of the same flow path. However, this method requires the calculation of far more streamlines to achieve plausible results (i.e., 122025, if all the area under grounded ice is used).

Although both these methods achieve similar results, the impact of random number sampling meant that the second method - calculating all flowlines from cells beneath the grounded ice - is recommended.

The mean ε_{Nd} values at a given cell at the ice sheet margin were then taken to reflect integration of the subglacial detritus along the flow lines. This approach does not account explicitly for detritus transport in subglacial hydrological networks, but these are unlikely to deviate significantly from ice flow vectors at the spatial scales of interest here.

https://doi.org/10.5194/gmd-2023-8
Preprint. Discussion started: 17 March 2023

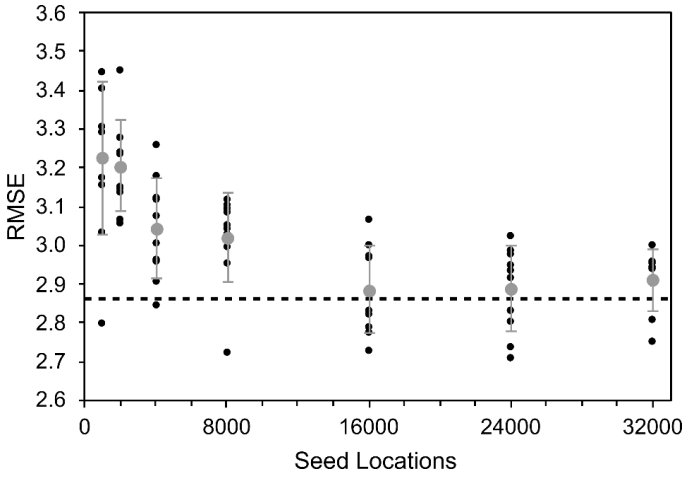

Figure 5. Impact on root mean square error (RMSE) mismatch associated with random number generation and number of seed locations. RMSE of 10 runs with different random number sets at 1000, 2000, 4000, 8000, 16000 and 32000 seed locations. The mean and standard deviation of the 10 runs are shown in grey. Different random number sets were generated using the MATLAB 'rng shuffle' function, which uses the time to simulate randomness. The dashed line indicates the results when using weighted flowlines generated at all points beneath the ice sheet (i.e. method 2).

By using a script external to the model code, this approach provides flexibility, with the opportunity to apply it to various existing model experiments. Our approach is not model-specific and could be applied to any ice sheet model output, providing key variables (bed elevation, basal shear stress and basal ice velocities with horizontal directional components) are saved.

4. Detritus Transport in the Ocean

Most sediment provenance records are from sites that are not located directly adjacent to the ice sheet margin. Transport of glaciogenic detritus in the ocean must therefore be considered. Here, methods of marine detritus transport are split into three key processes: iceberg rafting, bottom current transport, and gravitational downslope processes.

4.1 Iceberg Rafting

Iceberg rafted debris is one mechanism capable of long-distance transport of glaciogenic detritus in the ocean. Iceberg paths are a function of surface ocean current velocity, wind velocity and iceberg size, but surface current velocity dominates, particularly for large icebergs (Rackow et al., 2017; Wagner et al., 2017). The ORAS5 ocean velocity reanalysis dataset (Zuo et al., 2019) was thus used to approximate the pathways icebergs would be expected to take. The dataset extends to 80°S, which reaches the coast in most locations except portions of the Ross and Weddell seas. Simply interpolating available surface ocean velocities did not produce plausible flow directions near the ice sheet margin in the regions not covered by the reanalysis product. Consequently, the mean of the interpolated ocean velocity data and extrapolated ice velocities beyond the ice sheet margin was used, after scaling the latter to the mean of local ocean velocities so they are a consistent order of magnitude.

https://doi.org/10.5194/gmd-2023-8
Preprint. Discussion started: 17 March 2023


Geoscientific Model Development Discussions

A major simplification in our treatment of iceberg rafting of debris is our use of a constant debris load and distribution in all icebergs. In reality, the glaciological setting will strongly influence this. For instance, due to a relatively high number of rock outcrops, smaller icebergs calved from glaciers draining through the Transantarctic Mountains or mountainous parts of the Antarctic Peninsula certainly carry more englacial and supraglacial debris than larger tabular icebergs calved from the Ross or Filchner-Ronne ice shelves, which may predominantly carry basal debris (e.g., Anderson, 1999). The difficulty in quantitatively estimating iceberg debris distribution led to the simplifications discussed below, but we acknowledge that accounting for a variable debris load would improve the accuracy of the results.

To estimate the route of icebergs, the ocean surface current velocities are used as an input for the MATLAB streamline function, with the start locations set as the end point locations of the ice sheet provenance tracing component. If using the random number seed generation method (1), an end point of multiple terrestrial streamlines will be used as a start point for the equivalent number of times, weighting the relative amounts of sediment offshore to areas with the greatest terrestrial sediment flux. If using the 'all flowline' method (2), the original erosion rate values, summed at the ice sheet margin, are used to weight sediment flux. To reduce run time and computational cost by reducing the number of ocean surface velocity streamlines calculated, we also reduced the precision of the streamline function to the model grid resolution by rounding all start locations (i.e. terrestrial end locations) to the cell centre.

Sea ice variability and weather patterns create substantial seasonal and interannual variations in iceberg pathways estimated from ocean surface current velocities. To account for this effect, the surface ocean component was run 324 times, once for each month in the ocean reanalysis data spanning 1993 to 2019 (25 years). Experiments on the number of months required showed using additional years improved the match between seafloor surface sediment data and our predictions, plateauing beyond ~20 years. Our iceberg pathways are broadly similar to observed iceberg tracks and studies modelling iceberg drift and distribution (Fig. 6). In addition, the spatial distribution of smaller icebergs observed from ships matches with the distribution we produce (Orheim et al., 2021). Trajectories are not consistent from ~90°E westward to ~60°W, because the path of the Antarctic Coastal Current strays outside of our model domain (and study area) at ~90°E (Fig. 6). A larger domain would therefore be required to study areas between 90°E and 60°W (e.g. Iceberg Alley in the Weddell-Scotia confluence).

https://doi.org/10.5194/gmd-2023-8
Preprint. Discussion started: 17 March 2023

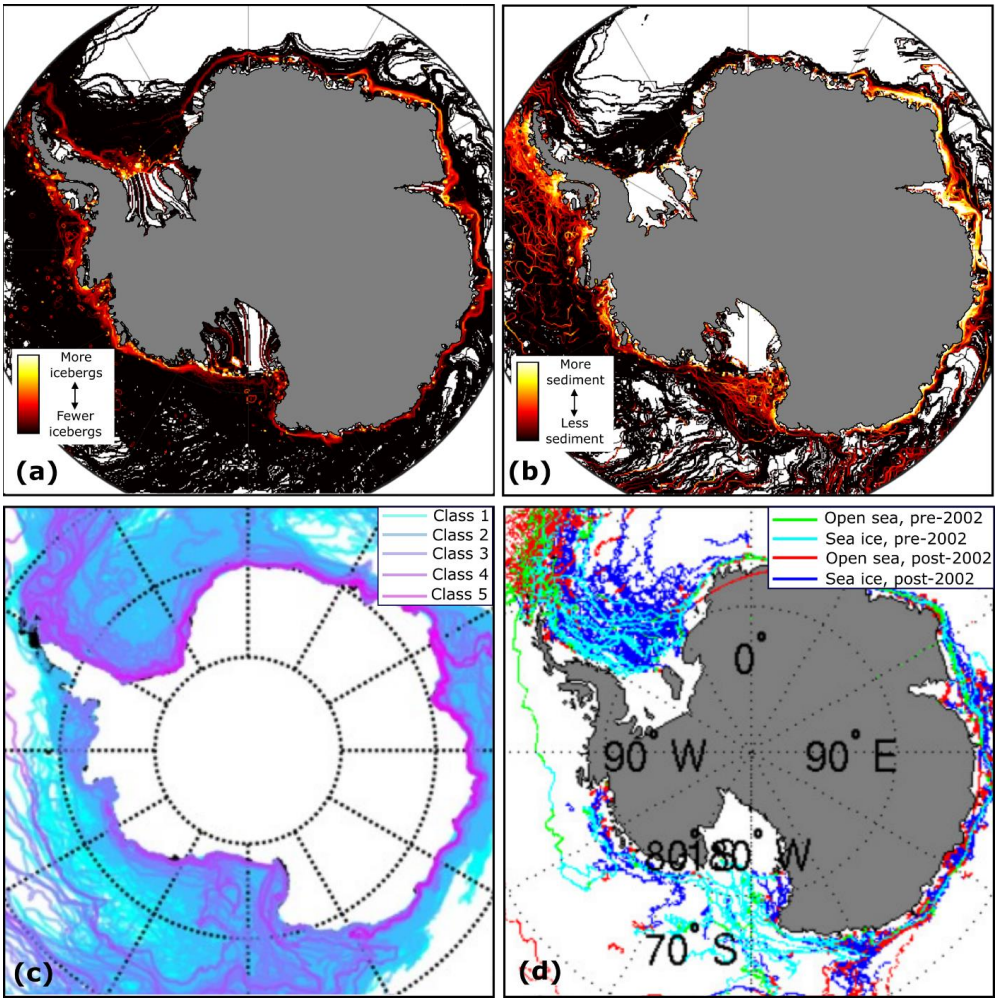

Figure 6. a) Heatmap of ocean surface velocity paths, which are assumed to approximate iceberg paths. 'Hotter' colours highlight areas where icebergs pass through more frequently. b) The relative quantity of iceberg-rafted sediment deposited by our representation of icebergs (unitless). c) Modelled iceberg trajectories accounting for additional influences such as wind velocities and sea ice (Rackow et al., 2017). Colours represent different iceberg size classes (1 = 0-1 km^2, 2 = 1-10 km^2, 3 = 10-100 km^2, 4 = 100-1000 km^2 and 5 = his1000-5000 km^2). d) Observed trajectories of large (>5 km across) icebergs from the U.S. National Ice Centre and Brigham Young University (Stuart and Long, 2011), presented in Tournadre et al. (2016). The broad pattern of iceberg movement produced by our algorithm in (a) agrees well with modelled (c) and observed (d) iceberg trajectories in our study area.

It is not realistic to assume that the volume of debris dropped by an iceberg remains constant over time. Transport of iceberg rafted debris (IBRD) over many hundreds of kilometres is possible (Dowdeswell et al., 1995), but typically transport is more local. This is because most glaciogenic debris is concentrated in the basal layers of the ice column, typically the lowermost 2-15 metres (Gow et al., 1979; Christoffersen et al., 2010; Shaw et al., 2011; Pettit et al., 2014). Ice sheet basal conditions, particularly melting/freezing rates, govern the

https://doi.org/10.5194/gmd-2023-8
Preprint. Discussion started: 17 March 2023

thickness and nature of this basal debris-rich layer, meaning conditions at the ice sheet bed will strongly influence the thickness and distribution of debris-rich ice (Dowdeswell and Murray, 1990). Consequently, there are substantial variations in entrained debris thickness around Antarctica even before the ice reaches the grounding zone. These complexities mean estimating a spatially variable debris distribution in the ice column around Antarctica is beyond the scope of this study.

Once in contact with the ocean, the debris-rich basal ice layer may begin to melt. Melt rates are particularly high along the coast of the Pacific sector of West Antarctica, where warm deep water upwelling onto the continental shelf reaches the ice sheet (e.g., Paolo et al., 2015). In many locations around Antarctica, melting of basal ice may begin before icebergs calve due to the presence of floating ice shelves. Melting at the grounding zone can lead to high accumulation of frozen-on basal debris or deforming subglacial till in sedimentary landforms, such as a till delta or grounding-zone wedge (e.g., Alley et al., 1989; Batchelor and Dowdeswell, 2015). Important influences on sub-ice shelf sedimentation include the size and morphology of the ice shelf, the presence of pinning points which can allow freeze on of new sediment, and the amount of relatively warm ocean water reaching the base of the floating ice which governs basal melt/freezing rates (e.g., Smith et al., 2019). These processes often lead to basal detritus being deposited, although debris near the base can also rise in the ice column if net freezing and/or surface ablation occur (Kellogg & Kellogg, 1988; Kellogg et al., 1990; Nicholls et al., 2012). To estimate sub-ice shelf melting, TASP uses the sub-ice shelf melt rates of Adusumilli et al. (2020) averaged over 2010-2018. Ice velocities are effectively treated as very slow ocean velocities, allowing a realistic amount of melting (and freezing) beneath the ice shelves.

Once icebergs have calved, melt rates in our algorithm are based on sea surface temperatures (T_s) corresponding with the monthly ocean surface velocity data used (Zuo et al., 2019). Melt rate will vary as a function of ocean temperature; we parameterise this from the empirical equation of Russell-Head (1980):

$$M_b = 2.08 \times 10^{-7}(T_s + 1.8)^{1.5} \quad (3)$$

Input of typical Southern Ocean sea surface temperatures into this equation and the assumption of a few metres of debris-rich basal ice provide debris yields comparable to those of studies with a more rigorous treatment of iceberg movement and melt (Dowdeswell and Murray, 1990; Hopwood et al., 2019).

The relative amount of debris release over time from individual icebergs will depend on iceberg size and frequency of overturning, and as such may be episodic (Drewry and Cooper, 1981; Dowdeswell, 1987; Dowdeswell and Murray, 1990). The debris distribution within the ice column is also important, with the amount of debris lost from an iceberg controlled by the thickness of the basal debris-rich ice layer and the relative concentration of debris. However, few data are available to suggest the relationship between debris concentration and depth in the ice column. Empirical relationships have been formulated, showing – from the base upwards - a constant debris content for several meters followed by a sharp exponential decay (Yevteyev, 1959), but very few data are available to suggest how typical this relationship is around Antarctica (Drewry and Cooper, 1981). Indeed, it can be assumed to vary significantly between localities depending on factors such as how the debris is incorporated (i.e. shearing and ice deformation vs. basal freeze on; Drewry and Cooper, 1981). To acknowledge these potential differences and investigate the sensitivity of our model to the distribution of basal debris, different relationships between basal debris concentration and depth were tested. A linear

https://doi.org/10.5194/gmd-2023-8
Preprint. Discussion started: 17 March 2023

relationship between debris yield and height above the ice base is therefore viewed as representative on the longer spatial and temporal scales of interest here. From an initial debris content at the ice-bed interface (D_0), the debris concentration in the basal ice (D) is given by:

$$D = D_0(1 - \frac{m}{Z}) \quad (4)$$

Where Z is the debris-rich basal ice thickness in metres and m is the current thickness of basal ice melted. m is the cumulative product of melt rate and the amount of time elapsed. This is only valid when the debris-rich basal ice layer is still present. Refrozen ice is treated as debris-free as the ice is floating. As only relative amounts of debris are relevant, $D_0 = 1$. Experiments were also performed with an exponential decline in debris yield and constant debris yield, but these had little impact on the overall result. The exponential relationship used is:

$$D = D_0 \exp(-\lambda \frac{m}{Z}) \quad (5)$$

Where a decay coefficient $\lambda = 5$ was selected to rain-out of basal debris for a length of time which agrees with more in-depth studies (e.g. Hopwood et al., 2019). Experiments were also performed with constant basal debris yield from the basal ice (i.e. $D = D_0$ while $m < Z$). These changes to debris distribution within the ice had a negligible impact on results.

As discussed above, the thickness of the basal debris-rich ice layer is variable around Antarctica so was tuned with the range of observed thicknesses (2-15 m) and our results compared with seafloor surface sediment data. This gave the lowest RMSE when using a thickness of 2 m for the basal debris layer. However, the overall result was relatively insensitive to the chosen value and given that observed debris-rich basal ice thicknesses are typically >2 m (Gow et al., 1979; Christoffersen et al., 2010; Shaw et al., 2011; Pettit et al., 2014), a value of 4 m was selected.

Supraglacial debris is very rare, but occasionally present in Antarctica (e.g., Evans and Ó Cofaigh, 2003), and englacial debris above basal debris-rich layers has also been observed (e.g. Nicholls et al., 2012; Winters et al. 2019; Smith et al., 2019). To account for a small supraglacial/englacial debris load and observed and theoretical transport of IBRD for hundreds to thousands of kilometres offshore (Dowdeswell and Murray, 1990; Dowdeswell et al., 1995; Gil et al., 2009), it is assumed there is a very small, but finite, debris yield for the entire iceberg track. This is set to 10^{-5} times the maximum debris load at the base of the ice column based on an assumption of a ~10% debris concentration in basal ice vs. ~0.001% higher in the ice column (Dowdeswell and Murray, 1990).

To produce an estimate of ε_{Nd} from iceberg rafting, the mean ε_{Nd} value of glaciogenic debris at the ice sheet margin was applied along the iceberg paths, and weighted relative to the amount of IBRD carried. This means debris from icebergs more proximal to their source location will dominate the ε_{Nd} signature, but where more local icebergs are absent, there is the potential for far-travelled icebergs to influence ε_{Nd} values of the seafloor sediments. After all pathways had been traced, the mean ε_{Nd} value was taken for each cell. Areas with no iceberg tracks over them, but within 40 km of an iceberg track, were filled using interpolation. This interpolation somewhat accounts for the potential for variations in ocean surface currents which are unresolved here. Furthermore, it is likely that over the decades to centuries integrated within most sediment samples of

https://doi.org/10.5194/gmd-2023-8
Preprint. Discussion started: 17 March 2023

centimetre-scale thickness, there would be transport of icebergs over more of the seafloor than captured in the 25 years of data used here.

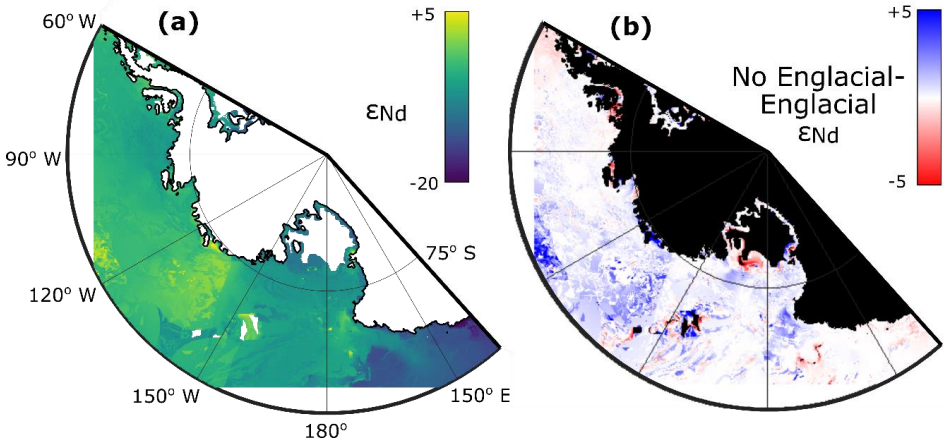

590 **Figure 7. Impact of assuming all debris is contained in a basal layer. a) The result assuming there is no englacial debris. b) Difference between the best match estimate ε_{Nd} values assuming englacial debris is absent (i.e. panel a) or present (i.e. Fig. 11g). Black indicates a lack of data.**

Including a very low minimum 'englacial' debris yield (i.e. debris above the basal ice) led to subtle differences
595 in the results (Fig. 7). In addition to representing detritus higher up in the ice column, this incorporation of a baseline debris yield may also help reflect the transport of very fine grained IBRD settling through the water column, which should track ocean flow patterns. Once released from the ice, silt particles (on the order of 5-50 μm) with slower settling velocities will be transported horizontally as they sink down through the water column over periods of days to months, leading to potential transport distances of tens to thousands of kilometres,
600 depending on grain size (Azetsu-Scott and Syvitski, 1999).

Fine-grained detritus can also derive from meltwater plumes rising from beneath the ice shelf base and/or the grounding zone (e.g. Lepp et al., 2022). These can deposit sediment tens of kilometres away from the grounding line and will track ocean currents (e.g. Smith et al., 2019, and references therein). Although meltwater plumes can travel at varying heights in the water column, depending on the relative densities of the plume and
605 surrounding ocean water, by using both surface and bottom current approximations, we assume their transport pathways are largely accounted for.

Given that our ε_{Nd} value estimate using ocean surface currents represents not only IBRD, but also settling of fined grained debris derived from icebergs or meltwater plumes, we hereafter refer to the estimate derived from this method as the 'surface current' method rather than the IBRD method.

610 Sea ice conditions impact iceberg movement and melt, leading to seasonally changing detritus transport in surface currents. We do not explicitly account for sea ice movement but note that the far lower sea surface temperatures in the winter months, when icebergs usually calve less frequently and are frozen into sea ice, will realistically weight our analyses towards the summer months.

https://doi.org/10.5194/gmd-2023-8
Preprint. Discussion started: 17 March 2023


Geoscientific Model Development Discussions

4.2 Bottom Currents

Iceberg rafting, and the processes described above, are not responsible for all transport of glacimarine detritus. One key process operating, especially on the continental rise, is the transport and deposition of predominantly silt- and clay-sized detritus by bottom currents. These currents typically flow parallel to the continental slope where they can influence the movement of detrital particles already in suspension. Bottom currents do not only deposit sediments as "contourites" but can also erode and redistribute particles from the seabed surface if their velocities are sufficiently high. As well as in the deep ocean, bottom current velocities can occasionally be sufficiently high to remobilise sediment on the continental shelf (Ha et al., 2014; Jenkins et al., 2018).

Bottom currents were defined as the deepest velocity in the ocean reanalysis product (Zuo et al., 2019). Due to very sparse in-situ measurements, knowledge of bottom current flow around the Antarctic margin is mainly derived from other oceanographic data, but we suggest the ocean reanalysis product provides the best estimate available. In TASP, detritus entrained in bottom currents is again routed using the MATLAB 'streamline' function. As ε_{Nd} values are generally measured on the <63 μm grain size fraction, it is assumed a current velocity of ~0.15 m/s is needed to start the resuspension and redistribution of the finest sediment particles (McCave and Hall, 2006; Gross and Williams, 1991). This threshold can vary significantly depending on properties such as the mean grain size, sorting and cohesivity of the sediment, but the 0.15 m/s approximation is assumed to be sufficient for our purposes.

The ocean reanalysis velocity data are unlikely to capture the full variability in bottom current dynamics, which include significant changes in current speed and orientation on timescales as short as hours (e.g. Camerlenghi et al., 1997; Giorgetti et al., 2003). This poses the question as to whether the sedimentary record reflects predominantly an integrated mean of long-term bottom-current flow variability, or whether it is dominated by episodes of peak current speed and current direction at these times. Here, it is assumed the latter case applies and, to account for the temporal variability in bottom current strength, peak flow velocities are assumed to be 2.5 times the monthly mean in the ocean reanalysis product. This relationship is based on measurements of bottom current strength at mooring sites around a contourite drift on the western Antarctic Peninsula continental rise (Camerlenghi et al., 1997; Giorgetti et al., 2003), which record peak velocities approximately two to three times greater than mean velocities. The bottom current speed record from the Antarctic Peninsula drift is also comparable with other bottom current records (Gross and Williams, 1991). It is therefore suggested that, in areas where mean flow velocity exceeds 0.06 m/s in the reanalysis product, the aforementioned 0.15 m/s threshold speed for the start of resuspension and winnowing is exceeded during times when currents are strongest. Consequently, all areas where bottom current velocities exceed 0.06 m/s are used as source locations for debris. Our approach is supported by the fact that the sortable silt mean size of seafloor surface sediment from another Antarctic Peninsula drift, recovered at a comparable water depth as the mooring measurements, suggests formation under a bottom current with a flow velocity matching the peak speed recorded in the mooring data (Hillenbrand et al., 2021).

As suspended particles will not be deposited uniformly over a given flow pathway, deposition over a streamline must be approximated. Although detailed modelling of bottom current erosion, transport and deposition is

https://doi.org/10.5194/gmd-2023-8
Preprint. Discussion started: 17 March 2023


Geoscientific Model Development Discussions

beyond the scope of this study, an approximation produces a realistic exponential decay in suspended particle concentration (c) over time (t_s, seconds):

$$c = c_0 \exp\left(-\frac{p t_s v_s}{y}\right) \quad (6)$$

Here, p is the probability of a particle sticking to the ocean floor, v_s is settling velocity, and y is the thickness of the layer with suspension load in metres (Einstein and Krone, 1962). As we are not concerned with absolute amounts of sediment, the initial particle concentration (c_0) can be neglected. A value of 3.3×10^{-4} m/s is used for the settling velocity, which is within the range expected for fine-grained detritus (Einstein and Krone, 1962; McCave, 2005). On the Antarctic margin, particles are often suspended in a nepheloid layer with a thickness on the order of ~10^2 – 10^3 m (e.g. Tucholke, 1977; Gilbert et al., 1998) instead of a layer with a clearly defined upper surface, making y a poorly constrained variable.

Low suspended particle layer thicknesses (y < 5 m) lead to very short transport distances, which are unlikely to capture bottom current transport; results instead resemble the surface current map used to initialise the bottom current flow paths. For longer transport distances, the large (100+ m) suspended layer thicknesses again show a better match with the provenance of recent seafloor surface sediments than intermediate thicknesses. This may be linked to these estimates having a longer detritus transport distance path and therefore estimated ε_{Nd} values with a larger spatial coverage. The lower RMSE may therefore be a result of having more mechanisms to choose from at more core sites, rather than a true improved match. Consequently, a thickness of 15 m is favoured as this is large enough to represent significant bottom current transport, but small enough to represent reasonable transport distances.

Although 15 m is substantially lower than the thickness of the nepheloid layer, we argue it is physically plausible given that nepheloid layer thicknesses have been measured in austral spring-summer, when the nepheloid layer probably contains large amounts of degrading biogenic matter (i.e. remnants of plankton blooms that took place just prior to these measurements). Furthermore, suspended particle concentrations are not uniform and are highest nearest the seafloor, and we are only concerned with bottom currents, which only comprise the lowermost part of the water column. Transmissometer data also suggest that suspended sediment concentrations increase markedly in the lower tens of metres of the water column (Gardner et al., 2020).

The probability of the particle sticking to the bed (p) in Eq. 6 can be calculated from bottom shear stress, τ_w (N m^{-2}), using a critical depositional stress, τ_c (N m^{-2}):

$$p = 1 - \frac{\tau_w}{\tau_c} \quad (7)$$

(Einstein and Krone 1962). τ_c is set to 0.08 N m^{-2}, in line with observed estimates for different classes of sediment which vary between 0.05 and 0.1 N m^{-2} (Shi et al., 2015; Lumborg, 2005; McCave, 2008). In turn, τ_w can be approximated as a product of vertically averaged velocity ($\bar{U}$) and water density (ρ) using a quadratic law (Mofjeld, 1988; Garcia and Parker, 1993):

$$\tau_w = \rho C_d \bar{U}^2 \quad (8)$$

At the deep water depths of interest here, the drag coefficient, C_d, can be estimated using:

https://doi.org/10.5194/gmd-2023-8
Preprint. Discussion started: 17 March 2023

Geoscientific Model Development Discussions

$$C_d = \kappa^2 / [\log\left(\frac{H}{z_0}\right) - 1]^2 \quad (9)$$

Where H is water depth and z_0 is the roughness length. Here we use 5×10^{-4} m for the roughness length, which is a reasonable approximation given that the drag coefficient is insensitive to small changes in this at large water depths (i.e. $H \gg z_0$) (Mofjeld, 1988). κ is the von Kármán constant, 0.41. This approximation yields a spatially-variable drag coefficient in the order of ~10^{-3}; a magnitude consistent with observations (Umlauf and Arenborg, 2009). For simplicity, the basal current velocity is assumed to be approximately equal to the depth-averaged velocity.

To set the initial ε_{Nd} composition of detritus mobilised by bottom currents, we use the output from the surface current method. To account for any seasonal changes in bottom current velocity, we then iterate the current tracing for 24 months (2018-2019 ocean reanalysis product), using the output from the previous month to set the ε_{Nd} value of sediment eroded where possible. Similar to the surface current estimate, the results for detritus moved by bottom currents is interpolated for 40 km around pathways. This helps account for unresolved pathways and for the fact that there is relatively little data to constrain modelled bottom current velocities in the ocean reanalysis product. Extending this interpolation distance gives a significantly better overall match with provenance data from the seabed surface sediments but, unlike the surface current estimate, there are fewer areas where bottom current remobilisation occurs. This means the improvement in the match with seafloor surface sediments is likely to be a consequence of having more mechanisms to choose from at some sites, rather than a more realistic result. Interpolating excessive distances from the modelled pathways will not represent the uncertainties described above, as in some areas bottom current velocities are unlikely to exceed the required threshold for sediment remobilisation. 40 km was therefore selected as a compromise between the representation of some uncertainty in bottom currents, whilst retaining some areas where bottom current remobilisation is unrealistic.

This approach is by necessity a major simplification of the treatment of particle transport and sediment remobilisation by bottom currents. Nevertheless, the areas subject to sediment remobilisation are captured, alongside the provenance of detritus reaching a given location through bottom current transport.

4.3 Gravitational Downslope Transport

Substantial volumes of glacimarine detritus can be moved through gravity-driven downslope processes, such as turbidity currents, slumps and debris flows. To represent these transport mechanisms, the mean ε_{Nd} values from the surface and bottom current methods at all locations with a slope of >1° (Stow, 1994), mostly confined to the continental slope, are selected. These grid cells are used as start locations from which the direction of gravitational transport is calculated by selecting the adjacent cell (including diagonals) with the lowest bed elevation. This next cell is set to the same ε_{Nd} value as the starting cell. This iterates until a cell is repeated (i.e., an upwards slope is reached). This method makes no attempt to account for travel distance along a gravitational transport pathway, but unlike ocean currents, such paths are unlikely to cross as the direction of travel will always be approximately perpendicular to the coast (on the shelf) or the shelf break (on the continental slope). Thus, calculation of the relative quantity of sediment is unnecessary.

https://doi.org/10.5194/gmd-2023-8
Preprint. Discussion started: 17 March 2023


Geoscientific Model Development Discussions

Bathymetric features not resolved at our 10 km model resolution mean gravitational flows are likely to carry detritus beyond the constraints of the approximate gravity flow paths. The gravitational transport ε_{Nd} estimate is therefore interpolated. Gravity flows do not necessarily shed their load once the slope falls below a threshold; mechanisms such as turbidity currents can carry particles over 1000 kilometres (e.g. Mulder, 2011). As our gravity flow paths were already typically 300-600 km long, we interpolate a further 300 km at all locations beyond the shelf break.

Theoretically, the relief on the continental shelf can be sufficient in places for gravity flows to redistribute sediment (e.g. Anderson et al., 1983; Hillenbrand et al., 2005). However, these processes are unlikely to transport significant amounts of sediment at the spatial scales (10's-100's km) considered here, and recent gravitational downslope deposits have only been identified locally on the very rugged, overdeepened inner continental shelf (e.g., Smith et al., 2009; Hogan et al., 2020). Thus, we do not interpolate the gravitational transport ε_{Nd} estimate on the continental shelf, defined as water depths <1200 m. Although this depth threshold is significantly deeper than the true average water depth of the shelf, which varies predominantly between ~400 and 500 m, using 1200 m avoids inclusion of most over-deepened areas on the innermost shelf close to the present ice sheet margin, where interpolation should be avoided. Very few sediment core sites exist on the upper continental slope, so using this depth threshold likely has little impact on our algorithm's results.

Turbidity currents flowing perpendicular to the shelf break down the continental slope can carry suspended particles to locations on the continental rise where they are captured by bottom currents flowing parallel to the margin, i.e. approximately parallel to the shelf break (e.g., Rodrigues et al., 2022a; Hillenbrand et al., 2021). To account for this interaction between gravitational downslope processes and bottom current transport, the output of the gravity flow method was iterated once with the bottom current method described above. This improves the match with observed surface sediment ε_{Nd} values. Although this approach does not explicitly represent material remobilised suspended by gravitational processes which is subsequently captured by bottom currents, using an iterative method accounts for particle transport both parallel and perpendicular to the continental margin in both the bottom current and gravitational ε_{Nd} value estimates.

4.4 Relative Contribution of Transport Mechanisms

A major challenge is apportioning the relative contribution of the three marine transport mechanisms described above around the Antarctic continental margin. In some settings, marine transport processes can be estimated given observations of geomorphological features (e.g., contourite drifts, channels eroded by turbidity currents), grain size parameters (e.g., content of coarse-grained clasts indicative of IBRD supply, percentage and mean of sortable silt as a proxy for bottom current vigour) and sedimentary structures (e.g., normally graded turbidites, winnowed layers of residual coarse-grained sediments). However, making these inferences requires good coverage with high-resolution bathymetric (and seismic) data and the collection of several sediment cores from targeted locations. Even then, however, it often remains difficult to determine the fraction of the sediment transported by different mechanisms (e.g., Rodrigues et al., 2022a, 2022b).

This issue is addressed by predicting a map of the provenance (ε_{Nd}) signature of detritus transported by each of the three key transport mechanisms at all sites where they are likely to impact detritus transport. Which mechanism, or combination of mechanisms, produces the closest match with observed seafloor surface sediment

https://doi.org/10.5194/gmd-2023-8
Preprint. Discussion started: 17 March 2023

Geoscientific Model Development Discussions

ε_{Nd} values at a given core site is then calculated. Mixtures of transport mechanisms are permitted where the measured surface sediment value lies between the different mechanism estimates. Assigning one method to each grid cell is not physically accurate, as all marine transport mechanisms may interact at a given location, with bottom currents (re-)distributing particles supplied by gravitational downslope processes or even reworking older sediments. Different mechanisms may also at some locations produce very similar ε_{Nd} values, which our approach does not account for. However, the approach used will indicate where different transport mechanisms are dominant. A major strength of this approach is that it does not require an estimate of the absolute quantity of detritus transported by each mechanism, which is useful given that the rates of these processes are poorly constrained.

5. Modelled Surface Sediment Signatures

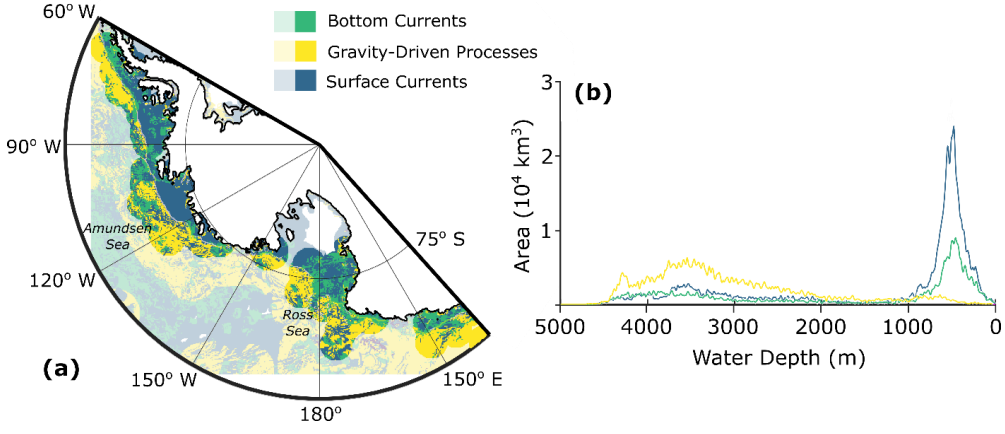

Figure 8. a) Applied transport mechanisms for glacimarine detritus providing the closest match with interpolated surface sediment ε_{Nd} values around the Antarctic continental margin. Colours are intense within 200 km of sample constraints, and pale away from these constraints. Grey shades show the (very limited) areas where two or more methods predict an identical ε_{Nd} value. b) The same data plotted against water depth (spline through 10 m bins), showing dominance of surface current estimate on the shelf and gravity driven processes beyond the shelf.

Predicting the ε_{Nd} values of seafloor surface sediments on the Antarctic margin from each of the three mechanisms and comparing these predictions to observations highlights that a single transport mechanism alone, such as iceberg rafting, cannot fully explain offshore sediment provenance. Each of the three mechanisms produces a close match with measured ε_{Nd} values in different areas (Fig. 8). On the continental shelf, the closest match between modelled and measured ε_{Nd} values is often provided by the surface current estimate. The results for the Amundsen Sea continental shelf in particular suggest a strong control of IBRD on the provenance of the sediments deposited there, likely due to slow bottom current speeds in the ocean reanalysis data. The Ross Sea, however, has some areas where the ε_{Nd} values predicted by bottom current transport most closely match observed seafloor ε_{Nd} values; these areas are concentrated around bathymetric highs, the Victoria Land coast, and parts of the outermost shelf/uppermost slope. There may be some relationship with the pathways of Ross Sea Bottom Water export, although the spatial match is not perfect (Orsi and Wiederwohl, 2009). Beyond the

https://doi.org/10.5194/gmd-2023-8
Preprint. Discussion started: 17 March 2023

Geoscientific Model Development Discussions
Open Access
EGU

continental shelf, gravitational downslope processes often provide the closest match to surface sediment ε_{Nd} values, suggesting sediment transport perpendicular to the shelf break is dominant further offshore.

https://doi.org/10.5194/gmd-2023-8
Preprint. Discussion started: 17 March 2023

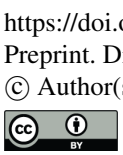

Geoscientific Model Development
Discussions
Open Access
EGU

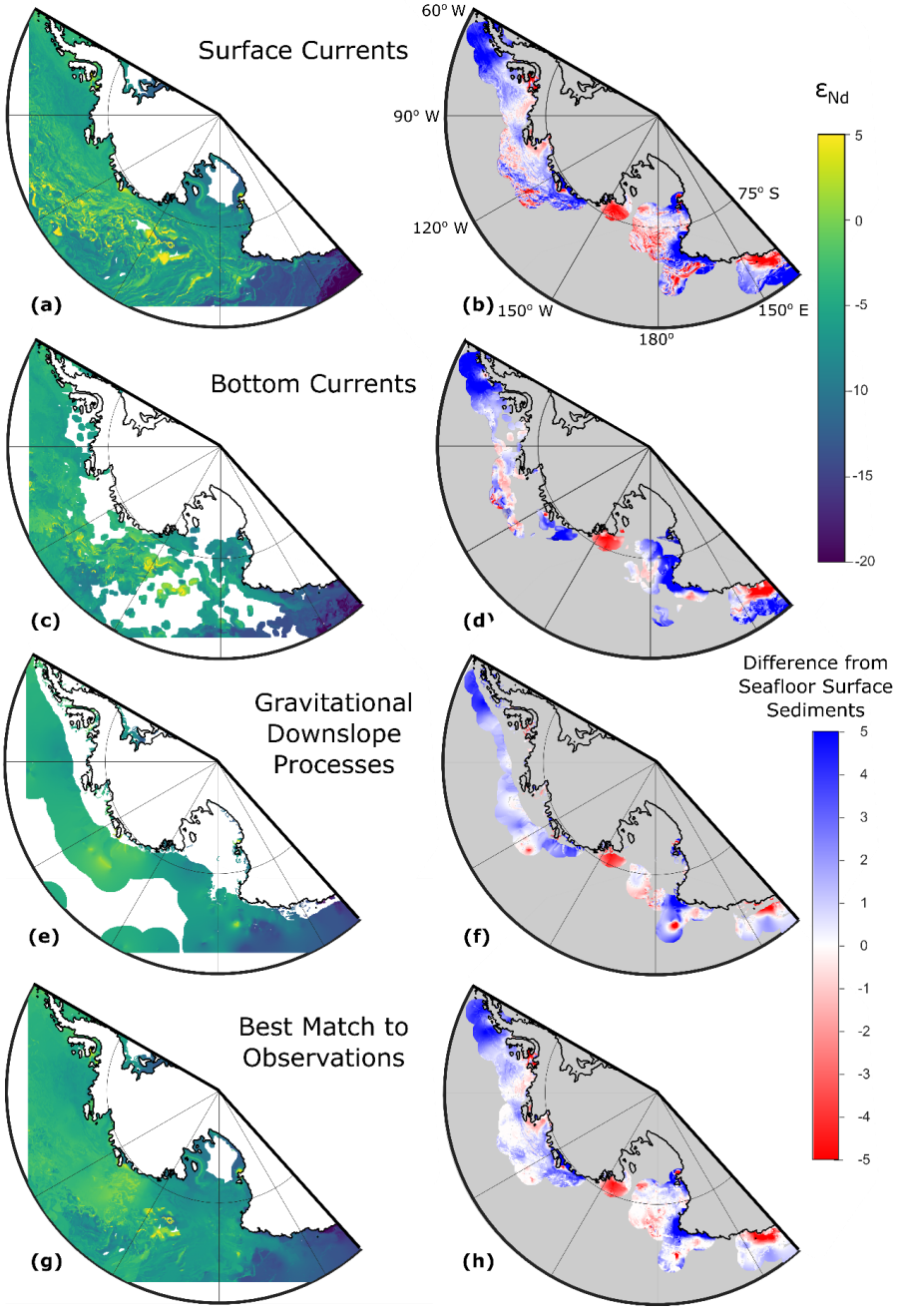

790 **Figure 9. Simulated ε_{Nd} values around the West Antarctic margin including the absolute values (a, c, e, g) and difference from the seafloor surface sediment data interpolation (b, d, f, h). The predicted ε_{Nd} provenance of seafloor surface sediments by modelled surface current (a & b), bottom current (c & d) and gravitational downslope (e & f) transport are shown, as well as the result when the closest matching method (surface current, bottom current, gravitational) to the interpolated core top ε_{Nd} values is selected for each grid cell (g and h).**

https://doi.org/10.5194/gmd-2023-8
Preprint. Discussion started: 17 March 2023

Near most surface sediment sample locations, we produce a close agreement between model results and measured data, with an overall root mean square error (RMSE) of 2.86 (Fig. 10). The algorithm's incorporation of marine detrital particle transport mechanisms results in a much closer match to ε_{Nd} values at seafloor sample sites compared to using a simple inverse distance weighting interpolation, which gives a RMSE of 3.77 when used to extrapolate the provenance signature of the glaciogenic detritus supplied to the ice sheet margin offshore (Fig. 11). This is because an inverse distance weighting method does not reflect transport of detritus parallel to the coast by ocean currents and therefore yields a worse match with surface sediment ε_{Nd} values.

Our algorithm's prediction matches 53% of surface sediment values within 1 epsilon unit and 82% within three epsilon units. The ε_{Nd} signals in published sediment provenance records off East Antarctica and in the Ross Sea exceed three epsilon units (e.g. Cook et al., 2013; Wilson et al., 2018; Marschalek et al., 2021). This implies our model predictions are sufficiently accurate at most sites to exceed the likely amplitude of changes in ε_{Nd} values caused by a change in the ice sheet drainage pattern or in areas of subglacial erosion and thus grounded ice-sheet extent.

https://doi.org/10.5194/gmd-2023-8
Preprint. Discussion started: 17 March 2023

Geoscientific Model Development Discussions

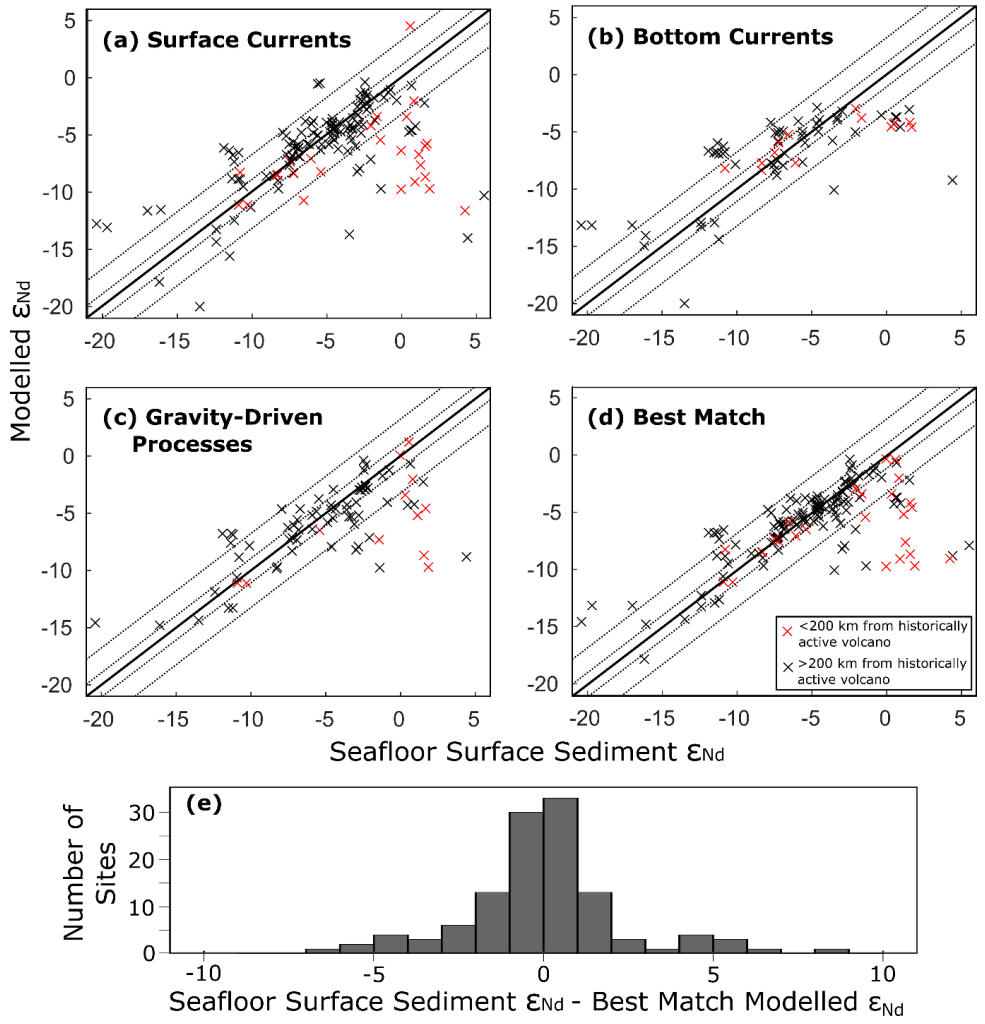

Figure 10. Comparison between observed and modelled ε_{Nd} values in seafloor surface sediments. Results are shown individually for each transport mechanism of glaciogenic detritus in the marine realm (a-c), plus selection of the nearest matching method (d). The solid 1:1 line is flanked by dotted lines indicating 1 and 3 epsilon unit deviations, respectively. Red crosses mark samples within 200 km of volcanoes which have been active in the historical observational era; these samples may (or may not) be influenced by volcanic material with a high (~+5) ε_{Nd} value. The difference between the measured and modelled (best match) ε_{Nd} values of seafloor surface sediments (d) is also shown as a histogram (e).

Broad spatial patterns in ε_{Nd} values and their match with measured surface sediments are generally consistent between the three transport mechanisms (Fig. 9). The surface current estimate is accurate in many areas close to the coast, with an overall RMSE of 3.57 (Fig. 9a,b; Fig. 10a). Further offshore, however, individual iceberg drift trajectories driven by surface current flow can be distinguished in the model ε_{Nd} output. At these locations, icebergs are less common, meaning our result often reflects a single iceberg trajectory rather than a mean of many drift paths as is the case closer to the continent. The strong, consistent imprint on iceberg drift of the

https://doi.org/10.5194/gmd-2023-8
Preprint. Discussion started: 17 March 2023

Antarctic Circumpolar Current (ACC) north of its southern boundary (SBACC; Fig 1) means different icebergs reaching a location north of the SBACC are likely to have a similar source; thus, there is a reduced need for multiple iceberg tracks over the same point. Despite this, a greater density of iceberg trajectories than that achieved by our algorithm is still required to reduce the gaps between the trajectories. The surface current method is therefore viewed as less reliable for predicting IBRD deposition in the deep ocean, where a surface current record spanning several decades and/or at a higher resolution would likely be required to get a denser network of iceberg trajectories over these areas, adding significant computational cost.

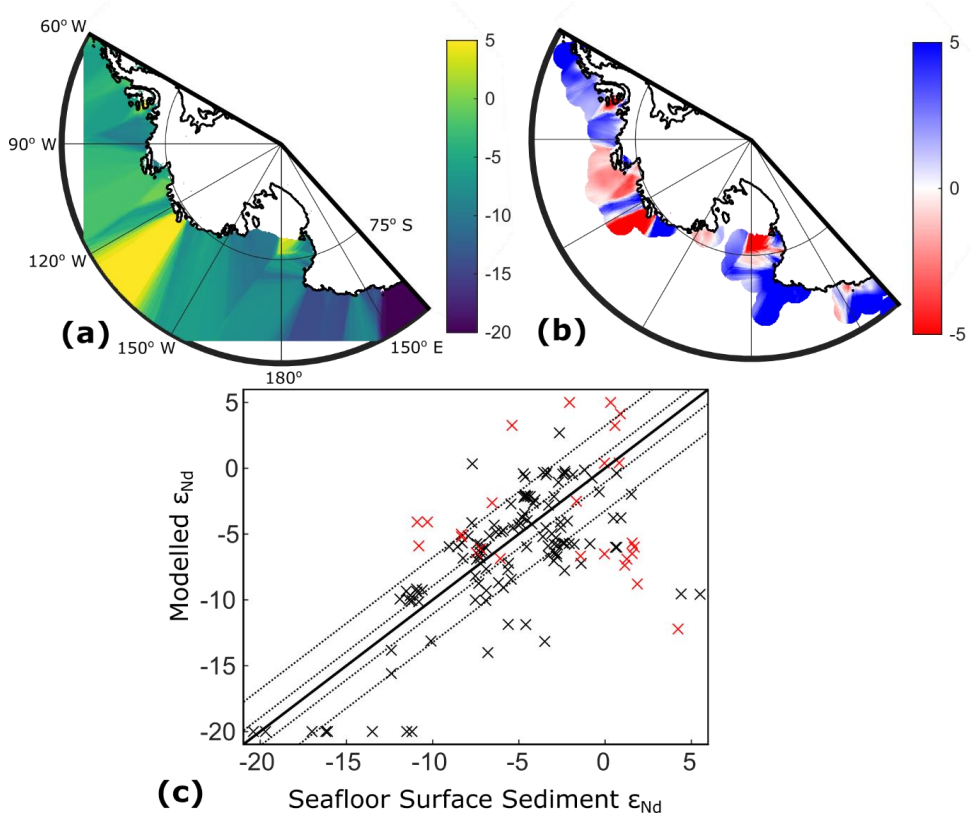

Figure 11. Results when using inverse distance weighting from the ice sheet margin for predicting ε_{Nd} values of seafloor surface sediments, including a) the extrapolated ε_{Nd} values and b) the difference between ε_{Nd} values predicted by this method and those measured on the surface sediments. c) Shows the scattered relationship between measured and modelled seafloor surface sediments.

Although the bottom current prediction of the ε_{Nd} sediment provenance also captures the same general patterns as the IBRD prediction, the bottom current estimate typically deviates more from measured ε_{Nd} values, with a RMSE of 3.90 (Fig. 9c,d; 10b). This seems to be linked to a general smoothing of the ε_{Nd} signal, which is consistent with this transport mechanism moving detritus that has already been mobilised or transported by a different mechanism, giving more potential for mixing. These results suggest bottom currents may dominate

https://doi.org/10.5194/gmd-2023-8
Preprint. Discussion started: 17 March 2023


Geoscientific Model Development Discussions

sediment provenance signals in relatively few areas, principally on parts of the continental slope and rise, where these bottom currents interact with suspended sediment particles supplied by downslope processes (Fig. 8).

The algorithm indicates that beyond the continental shelf, it is likely that the amount of detritus moved by gravitational downslope processes typically exceeds that of detritus solely supplied by ocean currents. Compared to the other transport mechanisms, modelled gravitational downslope transport gives the closest match with observations, with an RMSE of 3.09 (Fig. 9e,f; 10c). Substantial model-data mismatch for the gravitational downslope mechanism is limited to sites with special, localised environmental settings, which are discussed in detail below. The good agreement between our algorithm and seafloor surface samples beyond the shelf may also be partly explained by these ice-distal sediments typically containing more redeposited material. This makes the sediment here more mixed and integrated, leading to less extreme ε_{Nd} values with variations more likely to be averaged out. The ability of our model to closely reproduce ε_{Nd} values on the lower continental slope and the continental rise is probably linked to this smoothing of the ε_{Nd} signal. Due to a lack of geological constraints, our input ε_{Nd} map (Fig. 1) uses a mean value averaged for a particular rock type or a particular subglacial sediment type in several areas. This means heterogeneity in source ε_{Nd} values is reflected more directly on the continental shelf but is less relevant further offshore.

As well as the areas further offshore where gravitational downslope processes dominate, the model-data match is particularly good, and nearly always deviates by less than one ε_{Nd} unit, in the central Ross Sea and the Bellingshausen Sea (Fig. 9). In these areas, the close match is probably linked to the use of offshore data to inform the initial ε_{Nd} value map. However, the results in these areas nevertheless show that the assumptions made regarding rock distributions may be broadly correct and produce sensible results when TASP is applied to past ice sheet configurations.

The Amundsen Sea embayment offers a dense offshore sample network to compare our algorithm results to (Simões Pereira et al., 2018; 2020; Fig. 1a). The modelled ε_{Nd} values do not resolve finer-scale provenance features, but the match is good close to the terminus of both Pine Island and Thwaites glaciers and in the central Pine Island-Thwaites paleo-ice stream trough (Fig. 9). The algorithm prediction also broadly captures the mixing of the distinct detritus supplied by each of these two major WAIS outlets (Simões Pereira et al., 2020).

Areas where the three transport mechanisms consistently predict ε_{Nd} values that are less radiogenic (lower) than those observed include the coast of Victoria Land, part of the Hobbs Coast of Marie Byrd Land and the area around the northern tip of the Antarctic Peninsula (Fig. 9). This mismatch is likely attributable to volcanoes in these areas that are either still active or have been active in the recent past (e.g., Dunbar et al., 2021; Patrick and Smellie, 2013) (Fig. 1), as Cenozoic volcanic material in West Antarctica and Victoria Land is highly radiogenic (~+5.3 ε_{Nd}) and has a high Nd concentration (Goldich et al., 1975; Aviado et al., 2015; Futa and LeMasurier, 1983; Hart et al., 1997). This explanation is supported by the observation that clay-sized detritus in sediments offshore from the volcanic South Shetland Islands, near the northern tip of the Antarctic Peninsula, has a relatively high smectite content; this signal has a strong imprint on continental rise sediments in the region (e.g., Hillenbrand and Ehrmann, 2005; Hillenbrand et al., 2021).

Our methods do not make any attempt to account for tephra erupted above the ice surface and carried offshore, either by winds or in layers within icebergs, which could be present in the seafloor surface sediments in areas

https://doi.org/10.5194/gmd-2023-8
Preprint. Discussion started: 17 March 2023

close to and downwind of volcanoes and substantially influence ε_{Nd} values. Grain size distributions and visual observations in McMurdo Sound suggest that seafloor surface sediments there are dominated by (initially) airborne detritus that had been blown by strong winds both directly into the ocean and onto sea ice and the McMurdo Ice Shelf before being deposited on the seabed (Kellogg et al., 1990; Atkins and Dunbar, 2009), supporting this hypothesis. These observations show where marine sediment provenance records using ε_{Nd} values are likely influenced by radiogenic volcanic material; Nd isotope data from these areas should be interpreted with caution.

Three samples collected adjacent to the Adare and Hallett peninsulas on the Northern Victoria Land coast recorded particularly radiogenic ε_{Nd} values (Table 2), not captured by our algorithm. Visual mineralogical composition and ε_{Nd} values of >+4 suggest they consist almost entirely of detritus derived from the late Cenozoic volcanic rocks constituting these peninsulas. However, as the source volcanoes have not been active for at least ~2 million years (LeMasurier et al. 1990), this discrepancy cannot be attributed to recent tephra deposition but must result from the supply of locally eroded volcanic material. It instead highlights a limitation of our 10 km model resolution, which is not able to resolve such localised areas of a particular rock type (Fig. 1). If such sites close to the shore were of interest for sediment provenance tracing, a more localised, high resolution modelling approach would need to be pursued to yield more accurate results.

To visualise the locations of seafloor surface sediment samples which are in the vicinity of recently active volcanoes and therefore potentially influenced by significant volcanic deposition, sites within 200 km are highlighted in red in our scatter plots and excluded from our statistics (Fig. 10). We emphasise that the exclusion of these sites does not imply that sediment provenance data here are not useful; instead, the provenance data in these areas are viewed as having the potential for unaccounted-for volcanic influences. One exception is the recent volcanic activity suggested in the Hudson Mountains near Pine Island Bay in the eastern Amundsen Sea embayment (Patrick and Smellie, 2013; Corr and Vaughan, 2008), which we do not use to exclude data. Any volcanic input to marine sediments here is likely very local and minor given both the restricted geographical distribution of this tephra (Corr and Vaughan, 2008) and the large supply of non-volcanic glaciogenic debris from the adjacent Pine Island and Thwaites glaciers. For example, a petrographic analysis of coarse clasts >2 mm recovered in a box core in Pine Island Bay downstream of these two ice streams revealed that volcanic rocks accounted for only 0.5% of all the lithologies present (Lindow et al., 2016).

Volcanogenic detritus could also reach sample sites from volcanic seamounts and islands (Fig. 1). These range in age from the early Cenozoic to recent and are found offshore of Marie Byrd Land (Kipf et al., 2014; Hagen et al., 1998; Prestvik and Duncan, 1991; Hagedorn et al., 2007), north of Victoria Land (Johnson et al., 1982) and in the western Ross Sea (Lawver et al., 2012; Rilling et al., 2009; Panter and Castillo, 2007). Radiogenic isotope compositions are similar to the aforementioned Cenozoic volcanic rocks (Kipf et al., 2014; Panter and Castillo, 2007; Prestvik and Duncan, 1991). These seamounts and islands are not accounted for in our algorithm's predicted ε_{Nd} values for seafloor surface sediments as the extent and magnitude of the influence of such features is uncertain.

Offshore of the Wilkes Subglacial Basin and adjacent to the King Edward VII Peninsula, predicted ε_{Nd} values are more radiogenic (higher) than those measured in the seabed sediments (Fig. 13). A key factor influencing ε_{Nd} values in these regions is probably the supply of relatively radiogenic detritus via the Antarctic Coastal Current,

https://doi.org/10.5194/gmd-2023-8
Preprint. Discussion started: 17 March 2023

which in both these areas appears to be comprising a greater fraction of detritus in our model than reality. This is a result of icebergs remaining closer to the coast in the simulation. In these areas, we suggest that the ocean reanalysis product may not be resolving local factors - such as local ocean currents and the presence of grounded icebergs and fast ice - which lead to more far-travelled icebergs carrying relatively radiogenic detritus being diverted north, away from the coast. Offshore from Wilkes Subglacial Basin, for example, high-resolution modelling of sea ice trajectories around Mertz Glacier area shows that icebergs from the east are deflected north (Marsland et al., 2004), allowing locally derived debris to be more dominant in the lee side of the "Promontory" (Orejola et al., 2014). This area of deflection matches remarkably well with the area where model results and observations differ (red area, Fig. 12). Similarly, a gyre offshore from King Edward VII Peninsula deflects icebergs, which drift within the Antarctic Coastal Current westwards along the Amundsen Sea shelf, to the north before injecting them into the eastward flowing ACC (Keys, 1990; Rackow et al., 2017). This implies that grounded bergs, sea ice and unresolved ocean currents are a key control on the provenance of continental shelf sediments in these regions and should be carefully considered when interpreting sediment provenance records.

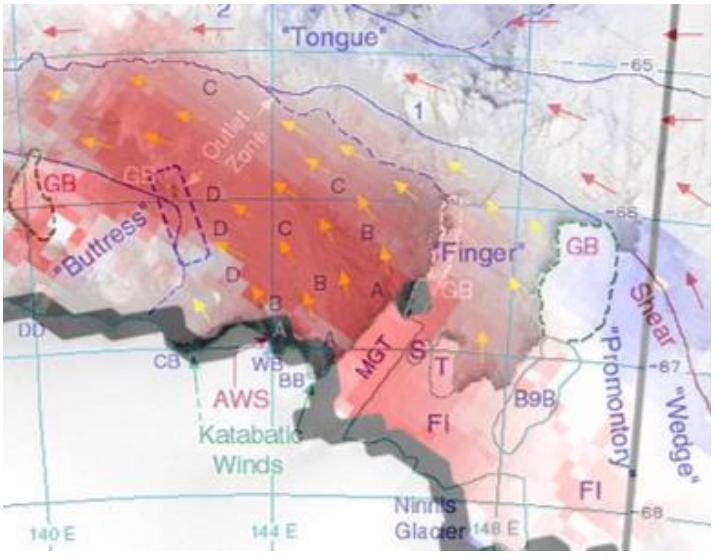

Figure 12. Close up of the Mertz Glacier Tongue (MGT) region imaged in June 1999, adapted from Massom et al. (2001) and Marsland et al. (2004). Red-blue colours indicate the discrepancy between the modelled and core top ε_{Nd} values as in Fig. 9h. Overlain is a map of old (multi-year) and new sea ice trajectories (red and yellow arrows, respectively), which are deflected to the north due to a "Promontory" of grounded bergs (GB), including iceberg B9B, and fast ice (FI). Note that the MGT had undergone a major calving event in 2010 but since then another seaward extending tongue consisting of floating glacial ice protruding from Ninnis and Mertz glaciers and amalgamated by fast ice has established (e.g., Wang et al., 2018). DD, Dumont d'Urville; CB, Commonwealth Bay; WB, Watt Bay; BB, Buchanan Bay. S and T are individual grounded bergs.

At some sites, disagreement observed may be linked to uncertain dating of seafloor surface sediments. To achieve a good spatial coverage, we group all available measurements likely to be late Holocene in age, but

https://doi.org/10.5194/gmd-2023-8
Preprint. Discussion started: 17 March 2023

difficulty in dating often carbonate-poor Antarctic sediments mean these may vary in age throughout the Holocene on a site-by-site basis.

6. Conclusions and Future Direction

We present the first computational method which predicts offshore sediment provenance around Antarctica using the results of ice sheet modelling and simple approximations of marine detrital particle transport mechanisms. Comparison to seafloor surface sediments helps understanding of the modern sedimentary system, including regions where different transport processes are likely more dominant, and regions where local factors such as sea ice or modern volcanism are likely impacting the neodymium isotope signature.

The TASP algorithm is particularly powerful beyond the continental shelf, where it produces a close match when using a simulation of the modern ice sheet to predict ε_{Nd} values for seafloor surface sediments. This is likely because greater integration of provenance signals makes our approach less reliant on precise mapping of uncertain subglacial geology. On the continental shelf, we capture the general pattern of ε_{Nd} values seen around West Antarctica and the East Antarctic George V Land margin. Any sites with substantial model-data disagreement can readily be explained by specific regional factors or geological uncertainties not captured in the provenance tracing.

The development of the TASP algorithm will permit application to simulations of palaeo ice sheets. These data will help interpret existing and future sediment provenance records by suggesting what ice sheet configurations could produce the changes in ε_{Nd} values seen at any given core site. Tighter coupling of numerical ice sheet model simulations and provenance data offers the potential for the advancement of both fields; results of numerical modelling can be directly compared to real-world constraints, and interpretations of geochemical data can be tested and visualised.

Improved knowledge of subglacial geology, particularly in much of the West Antarctic interior, would enable TASP to produce even more useful and accurate results. Future geophysical surveys, as well as drilling campaigns targeting subglacial sediments and especially bedrock, will reduce uncertainty in our ε_{Nd} map and thus predictions offshore. Additional insights could be achieved by expanding this approach to different parts of the Antarctic continent. Our method could also be adapted for numerous provenance proxies, each offering a different sensitivity to changes to erosion thus different precision in different regions and at different times in the past (Licht and Hemming, 2017). Such proxies include detrital mineral dating, major and trace element geochemistry, clay and heavy mineralogy, or clast petrography.

https://doi.org/10.5194/gmd-2023-8
Preprint. Discussion started: 17 March 2023

Geoscientific Model Development Discussions

Code Availability

The source code is available on the Git repository https://github.com/jwm17/TASP (DOI: 10.5281/zenodo.7529996). Additional files created for this study and required to execute the code are also found there.

Data Availability

Data for melt rates beneath modern ice shelves (Adusumilli et al., 2020) can be downloaded here: DOI:10.6075/J04Q7SHT. The ORAS5 ocean reanalysis product files used at a quarter degree resolution (velocity and sea surface temperature) can be downloaded here: DOI:10.24381/cds.67e8eeb7.

The neodymium isotope composition data published here are available at DOI:10.5281/zenodo.7548284. ***Note that these data have been embargoed, but will be released before publication and are identical to those in Table 2.***

Author Contributions

JM, EG and TvdF designed the study. JM developed the code with assistance from EG. CDH and MS advised on sedimentological and glaciological aspects of the manuscript, respectively. LH collected the new Nd isotope data to complement existing published datasets.

Competing Interests

The authors declare that they have no conflict of interest.

Acknowledgements

JM and TvdF acknowledge funding from the NERC (DTP scholarship to JM, NE/L002515/1, and grants NE/R018219/1 and NE/W000172/1 to TvdF).

We would like to thank Tom Jordan for providing insight into subglacial geology in the Amundsen Sea sector based on unpublished data.

The Ross Sea surface sediments, from which new Nd isotope data were collected, were supplied by Helen Bostock from NIWA, Wellington, New Zealand.

https://doi.org/10.5194/gmd-2023-8
Preprint. Discussion started: 17 March 2023

References

Adusumilli, S., Fricker, H. A., Medley, B., Padman, L., and Siegfried, M. R.: Interannual variations in meltwater input to the Southern Ocean from Antarctic ice shelves, Nat. Geosci., 13, 616-620, doi:10.1038/s41561-020-0616-z, 2020.

Aitken, A. R. A., and Urosevic, L.: A probabilistic and model-based approach to the assessment of glacial detritus from ice sheet change, Palaeogeogr., Palaeocl. 561, 110053. doi:10.1016/j.palaeo.2020.110053, 2021.

Alley, R. B., Blankenship, D. D., Rooney, S. T. and Bentley, C. R.: Sedimentation beneath ice shelves—the view from ice stream B, Mar. Geol., 85, 101-120, doi:10.1016/0025-3227(89)90150-3, 1989.

Alley, R. B., Cuffey, K. M. and Zoet, L. K.: Glacial erosion: status and outlook, Ann. Glaciol., 60, 1-13, doi:10.1017/aog.2019.38, 2019.

Anderson, J. B. Antarctic marine geology. Cambridge University Press, doi:10.1017/CBO9780511759376, 1999.

Andrews, J. T., and LeMasurier, W.: Resolving the argument about volcanic bedrock under the West Antarctic Ice Sheet and implications for ice sheet stability and sea level change, Earth Planet. Sc. Lett., 568, 117035, doi:10.1016/j.epsl.2021.117035, 2021.

Armienti, P., Ghezzo, C., Innocenti, F., Manetti, P., Rocchi, S., and Tonarini, S.: Isotope geochemistry and petrology of granitoid suites from Granite Harbour intrusives of the Wilson Terrane, North Victoria Land, Antarctica, Eur. J. Mineralogy, 2, 103-124, doi:10.1127/ejm/2/1/0103, 1990.

Aviado, K. B., Rilling-Hall, S., Bryce, J. G., and Mukasa, S. B.: Submarine and subaerial lavas in the West Antarctic Rift System: Temporal record of shifting magma source components from the lithosphere and asthenosphere, Geochem., Geophy., Geosy., 16, 4344-4361, doi:10.1002/2015GC006076, 2015.

Azetsu-Scott, K. and Syvitski, J. P.: Influence of melting icebergs on distribution, characteristics and transport of marine particles in an East Greenland fjord, J. Geophys. Res-Oceans, 104, 5321-5328, doi: 10.1029/1998JC900083, 1999.

Batchelor, C. L., & Dowdeswell, J. A.: Ice-sheet grounding-zone wedges (GZWs) on high-latitude continental margins, Mar. Geol., 363, 65-92, doi:10.1016/j.margeo.2015.02.001, 2015

Bertram, R.A.: Reconstructing the East Antarctic Ice Sheet during the Plio-Pleistocene using Geochemical Provenance Analysis, Ph.D. thesis, Imperial College London, doi:10.25560/83552, 2018.

Bertram, R. A., Wilson, D. J., van de Flierdt, T., McKay, R. M., Patterson, M. O., Jimenez-Espejo, F. J., Escutia, C., Duke, G.C., Taylor-Silva, B.I. and Riesselman, C. R.: Pliocene deglacial event timelines and the biogeochemical response offshore Wilkes Subglacial Basin, East Antarctica, Earth Planet. Sc. Lett., 494, 109-116, doi:10.1016/j.epsl.2018.04.054, 2018.

Boger, S. D.: Antarctica—before and after Gondwana, Gondwana Res., 19, 335-371, doi:10.1016/j.gr.2010.09.003, 2011.

Borg, S. G., & DePaolo, D. J.: Laurentia, Australia, and Antarctica as a Late Proterozoic supercontinent: constraints from isotopic mapping, Geology, 22, 307-310, doi: 10.1130/0091-7613(1994)022<0307:LAAAAA>2.3.CO;2, 1994.

Borg, S. G., Depaolo, D. J., and Smith, B. M.: Isotopic structure and tectonics of the central Transantarctic Mountains, J. Geophys. Res-Solid Earth, 95, 6647-6667, doi:10.1029/JB095iB05p06647, 1990.

Burton-Johnson, A. and Riley, T. R.: Autochthonous v. accreted terrane development of continental margins: a revised in situ tectonic history of the Antarctic Peninsula, J. Geol. Soc. London, 172, 822-835, doi: 10.1144/jgs2014-11, 2015.

https://doi.org/10.5194/gmd-2023-8
Preprint. Discussion started: 17 March 2023

Camerlenghi, A., Crise, A., Pudsey, C. J., Accerboni, E., Laterza, R., and Rebesco, M.: Ten-month observation of the bottom current regime across a sediment drift of the Pacific margin of the Antarctic Peninsula, Antarct. Sci., 9, 426-433, doi:10.1017/S0954102097000552, 1997.

Christoffersen, P., Tulaczyk, S. and Behar, A.: Basal ice sequences in Antarctic ice stream: exposure of past hydrologic conditions and a principal mode of sediment transfer, J. Geophys. Res-Earth, 115, doi:10.1029/2009JF001430, 2010.

Cook, C. P., Hemming, S. R., van de Flierdt, T., Davis, E. L. P., Williams, T., Galindo, A. L., Jimnez-Espejo, F.J., and Escutia, C.: Glacial erosion of East Antarctica in the Pliocene: A comparative study of multiple marine sediment provenance tracers, Chem. Geol., 466, 199-218, doi:10.1016/j.chemgeo.2017.06.011, 2017.

Cook, C. P., van de Flierdt, T., Williams, T., Hemming, S. R., Iwai, M., Kobayashi, M., Jimnez-Espejo, F.J., Escutia, C., Gonxalez, J. J., Khim, B.-K., McKay, R.M., Passchier, S., Boharty, S.M., Riesselman, C.R., Tauxe, L., Sugisaki, S., Galindo, A.L., Patterson, M.O., Sangiorgi, F., Pierce, E.L., Brinkhuis, H., Klaus, A., Fehr, A., Bendle, J.A.P., Bilj, P.K., Carr., S.A., Dunbar., R.B., Flores, J.A., Hayden, T.G., Katsuki, K., Kong, G.S., Nakai, M., Olney., M.P., Pekar, S.F., Pross, J., Rohl, U., Sakai, T., Shrivastava, P.K., Stickley, C.E., Tuo, S., Welsh, K. and Yamane, M.: Dynamic behaviour of the East Antarctic ice sheet during Pliocene warmth, Nat. Geosci., 6, 765-769, doi:10.1038/ngeo1889, 2013.

Corr, H. F. and Vaughan, D. G.: A recent volcanic eruption beneath the West Antarctic ice sheet, Nat. Geosci., 1, 122-125, doi:10.1038/ngeo106, 2008.

Cox, S.C., Parkinson, D.L., Allibone, A.H. and Cooper, A.F.: Isotopic character of Cambro-Ordovician plutonism, southern Victoria Land, Antarctica, New Zeal. J. Geol. Geop., 43, 501-520, doi:10.1080/00288306.2000.9514906, 2000.

Cox S.C., Smith Lyttle B. and the GeoMAP team: SCAR GeoMAP dataset, GNS Science, Lower Hutt, New Zealand, release v.201907, doi:10.21420/7SH7-6K05, 2019.

Craddock, J. P., Schmitz, M. D., Crowley, J. L., Larocque, J., Pankhurst, R. J., Juda, N., Konstantinou, A. and Storey, B.: Precise U-Pb zircon ages and geochemistry of Jurassic granites, Ellsworth-Whitmore terrane, central Antarctica. Geol. Soc. Am. Bull., 129, 118-136, doi:10.1130/B31485.1, 2017.

Curtis, M. L., Leat, P. T., Riley, T. R., Storey, B. C., Millar, I. L. and Randall, D. E.: Middle Cambrian rift-related volcanism in the Ellsworth Mountains, Antarctica: tectonic implications for the palaeo-Pacific margin of Gondwana, Tectonophysics, 304, 275-299, doi:10.1016/S0040-1951(99)00033-5, 1999.

Dallai, L., Ghezzo, C., and Sharp, Z. D.: Oxygen isotope evidence for crustal assimilation and magma mixing in the Granite Harbour Intrusives, Northern Victoria Land, Antarctica, Lithos, 67, 135-151, doi:10.1016/S0024-4937(02)00267-0, 2003.

DeConto, R. M. and Pollard, D.: Contribution of Antarctica to past and future sea-level rise, Nature, 531, 591-597, doi:10.1038/nature17145, 2016.

Delmonte, B., Petit, J. R., Andersen, K. K., Basile-Doelsch, I., Maggi, V. and Ya Lipenkov, V.: Dust size evidence for opposite regional atmospheric circulation changes over east Antarctica during the last climatic transition, Clim. Dynam., 23, 427-438, doi:10.1007/s00382-004-0450-9, 2004.

Dowdeswell, J. A.: Processes of glacimarine sedimentation, Prog. Phys. Geog., 11, 52-90, doi: 10.1177/030913338701100103, 1987.

Dowdeswell, J. A., Maslin, M. A., Andrews, J. T., and McCave, I. N.: Iceberg production, debris rafting, and the extent and thickness of Heinrich layers (H-1, H-2) in North Atlantic sediments, Geology, 23, 301-304, doi:10.1130/0091-7613(1995)023<0297:IPDRAT>2.3.CO;2, 1995.

Dowdeswell, J. A. and Murray, T.: Modelling rates of sedimentation from icebergs, Geo. Soc. S. P., 53, 121-137, doi:10.1144/GSL.SP.1990.053.01.07, 1990.

Drewry, D. J. and Cooper, A. P. R.: Processes and models of Antarctic glaciomarine sedimentation, Ann. Glaciol., 2, 117-122, doi:10.3189/172756481794352478, 1981.

https://doi.org/10.5194/gmd-2023-8
Preprint. Discussion started: 17 March 2023

Dunbar, N. W., Iverson, N. A., Smellie, J. L., McIntosh, W. C., Zimmerer, M. J. and Kyle, P. R.: Active volcanoes in Marie Byrd Land, Geol. Soc. Mem., 55, 759-783, doi:10.1144/M55-2019-29, 2021.

Einstein, H. A. and Krone, R. B.: Experiments to determine modes of cohesive sediment transport in salt water, J. Geophys. Res., 67, 1451-1461, doi:10.1029/JZ067i004p01451, 1962.

Ehrmann, W., Hillenbrand, C. D., Smith, J. A., Graham, A. G., Kuhn, G. and Larter, R. D.: Provenance changes between recent and glacial-time sediments in the Amundsen Sea embayment, West Antarctica: clay mineral assemblage evidence, Antarct. Sci., 23, 471-486, doi:10.1017/S0954102011000320, 2011

Elliot, D. H., Fleming, T. H., Kyle, P. R. and Foland, K. A.: Long-distance transport of magmas in the Jurassic Ferrar large igneous province, Antarctica, Earth Planet. Sc. Lett., 167, 89-104, doi: 10.1016/S0012-821X(99)00023-0, 1999.

Elliot, D. H., Larsen, D., Fanning, C. M., Fleming, T. H. and Vervoort, J. D.: The Lower Jurassic Hanson Formation of the Transantarctic Mountains: implications for the Antarctic sector of the Gondwana plate margin, Geol. Mag., 154, 777-803, doi:10.1017/S0016756816000388, 2017.

Estrada, S., Läufer, A., Eckelmann, K., Hofmann, M., Gärtner, A. and Linnemann, U.: Continuous Neoproterozoic to Ordovician sedimentation at the East Gondwana margin—Implications from detrital zircons of the Ross Orogen in northern Victoria Land, Antarctica, Gondwana Res., 37, 426-448, doi:10.1016/j.gr.2015.10.006, 2016

Evans, J. and Cofaigh, C. Ó.: Supraglacial debris along the front of the Larsen-A Ice Shelf, Antarctic Peninsula, Antarct. Sci., 15, 503-506, doi:10.1111/j.1502-3885.2003.tb01443.x, 2003.

Farmer, G. L., Licht, K., Swope, R. J. and Andrews, J.: Isotopic constraints on the provenance of fine-grained sediment in LGM tills from the Ross Embayment, Antarctica, Earth Planet. Sci. Lett. 249, 90–107, doi:10.1016/j.epsl.2006.06.044, 2006.

Ferraccioli, F., Armadillo, E., Jordan, T., Bozzo, E. and Corr, H.: Aeromagnetic exploration over the East Antarctic Ice Sheet: a new view of the Wilkes Subglacial Basin, Tectonophysics, 478, 62-77, doi: 10.1016/j.tecto.2009.03.013, 2009.

Ferris, J., Johnson, A. and Storey, B.: Form and extent of the Dufek intrusion, Antarctica, from newly compiled aeromagnetic data, Earth Planet. Sc. Lett., 154, 185-202, doi:10.1016/S0012-821X(97)00165-9, 1998.

Fleming, T. H.: Isotopic and chemical evolution of the Ferrar Group. Beardmore Glacier region, Antarctica. Ph.D. thesis, Ohio State University, http://rave.ohiolink.edu/etdc/view?acc_num=osu1487929745335032, 1995.

Frederick, B. C., Young, D. A., Blankenship, D. D., Richter, T. G., Kempf, S. D., Ferraccioli, F. and Siegert, M. J.: Distribution of subglacial sediments across the Wilkes Subglacial Basin, East Antarctica, J. Geophys. Res.-Earth, 121, 790-813, doi:10.1002/2015JF003760, 2016.

Futa, K. and LeMasurier, W. E.: Nd and Sr isotopic studies on Cenozoic mafic lavas from West Antarctica - another source for continental alkali basalts, Contrib. Mineral. Petr., 83, 38-44, doi:10.1007/BF00373077, 1983.

Garcia, M. and Parker, G.: Experiments on the entrainment of sediment into suspension by a dense bottom current, J. Geophys. Res.-Oceans, 98, 4793-4807, doi:10.1029/92JC02404, 1993.

Garçon, M., Chauvel, C., France-Lanord, C., Huyghe, P. and Lavé, J.: Continental sedimentary processes decouple Nd and Hf isotopes, Geochim. Cosmochim. Ac., 121, 177-195, doi:10.1016/j.gca.2013.07.027, 2013.

Gardner, W.D., Mishonov A.V. and Richardson M.J.: Global Transmissometer Database V3, Ocean Data View, https://odv.awi.de/data/ocean/global-transmissometer-database/, 2020.

Gil, I. M., Keigwin, L. D. and Abrantes, F. G.: Deglacial diatom productivity and surface ocean properties over the Bermuda Rise, northeast Sargasso Sea, Paleoceanography, 24, doi:10.1029/2008PA001729, 2009.

Gilbert, I. M., Pudsey, C. J. and Murray, J. W.: A sediment record of cyclic bottom-current variability from the northwest Weddell Sea, Sediment. Geol., 115, 185-214, doi:10.1016/S0037-0738(97)00093-6, 1998.

https://doi.org/10.5194/gmd-2023-8
Preprint. Discussion started: 17 March 2023

Giorgetti, A., Crise, A., Laterza, R., Perini, L., Rebesco, M. and Camerlenghi, A.: Water masses and bottom boundary layer dynamics above a sediment drift of the Antarctic Peninsula Pacific Margin, Antarct. Sci.,15, 537-546, doi:10.1017/S0954102003001652, 2003.

Goldstein, S. L. and Hemming, S. R.: Long-lived isotopic tracers in oceanography, paleoceanography, and ice-sheet dynamics, Treatise on geochemistry, 6, 453-489, doi:10.1016/B0-08-043751-6/06179-X, 2003.

Golledge, N. R., Clark, P. U., He, F., Dutton, A., Turney, C. S. M., Fogwill, C. J. Naish, T.R., Levy, R.H., McKay, R.M., Lowry, D.P., Bertler., N.A.N., Dunbar, G.B. and Carlson, A. E.: Retreat of the Antarctic Ice Sheet during the Last Interglaciation and implications for future change, Geophys. Res. Lett., 48, e2021GL094513, 10.1029/2021GL094513, 2021.

Golynsky, A. V., Ferraccioli, F., Hong, J. K., Golynsky, D. A., von Frese, R. R. B., Young, D. A., Blankenship, D., Holt, J.W., Ivanov, S.V., Kiselev, A.V., Masolov, V.N, Eagles., G., Gohl, K., Jokat., W., Damaske, D., Finn, C., Aitken, A., Bell, R.E., Armadillo, E., Jordan, T.A., Greenbaum, J.S., Bozzo, E., Caneva, G., Forsberg, R., Ghidella, M., Galindo-Zaldivar, J., Bohoyo, F., Martos, Y.M., Nogi, Y., Quartini, E., Kim, H.R. and Roberts, J. L.: New magnetic anomaly map of the Antarctic, Geophys. Res. Lett. 45, 6437-6449, doi:10.1029/2018GL078153, 2018.

Goodge, J. W.: Geological and tectonic evolution of the Transantarctic Mountains, from ancient craton to recent enigma, Gondwana Res., 80, 50-122, doi:10.1016/j.gr.2019.11.001, 2020.

Goodge, J. W., Fanning, C. M., Norman, M. D. and Bennett, V. C.: Temporal, isotopic and spatial relations of early Paleozoic Gondwana-margin arc magmatism, central Transantarctic Mountains, Antarctica, J. Petrol., 53, 2027-2065, doi:10.1093/petrology/egs043, 2012.

Goodge, J. W. and Finn, C. A.: Glimpses of East Antarctica: Aeromagnetic and satellite magnetic view from the central Transantarctic Mountains of East Antarctica, J. Geophys. Res.-Earth, 115, doi:10.1029/2009JB006890, 2010.

Goodge, J. W., Vervoort, J. D., Fanning, C. M., Brecke, D. M., Farmer, G. L., Williams, I. S., Myrow, P.M. and DePaolo, D. J.: A positive test of East Antarctica–Laurentia juxtaposition within the Rodinia supercontinent, Science, 321, 235-240, doi:10.1126/science.1159189, 235-240, 2008.

Gow, A. J., Epstein, S. and Sheehy, W.: On the origin of stratified debris in ice cores from the bottom of the Antarctic ice sheet, J. Glaciol., 23, 185-192, doi:10.3189/S0022143000029828, 1979.

Gross, T. F. and Williams, A. J.: Characterization of deep-sea storms, Mar. Geol., 99, 281-301, doi:10.1016/0025-3227(91)90045-6, 1991.

Hagedorn, B., Gersonde, R., Gohl, K. and Hubberten, H. W.: Petrology, geochemistry and K/Ar age constraints of the eastern De Gerlache Seamount alkaline basalts (Bellingshausen Sea, southeast Pacific), Polarforschung, 76, 87-94, doi:10013/epic.28876.d001, 2007.

Hagen, R. A., Gohl, K., Gersonde, R., Kuhn, G., Völker, D., & Kodagali, V. N.: A geophysical survey of the De Gerlache Seamounts: preliminary results, Geo-Mar. Lett., 18, 19-25, doi:10.1007/s003670050047, 1998.

Haran, T., Bohlander, J., Scambos, T., Painter, T., and Fahnestock, M.: MODIS Mosaic of Antarctica 2008-2009 (MOA2009) Image Map, Version 1, NASA National Snow and Ice Data Center Distributed Active Archive Center [data set], doi:10.5067/4ZL43A4619AF, 2014, updated 2019.

Hart, S. R., Blusztajn, J., LeMasurier, W. E. and Rex, D. C.: Hobbs Coast Cenozoic volcanism: Implications for the West Antarctic rift system, Chem. Geol., 139, 223-248, doi:10.1016/S0009-2541(97)00037-5, 1997.

Hauptvogel, D. W. and Passchier, S.: Early–Middle Miocene (17–14 Ma) Antarctic ice dynamics reconstructed from the heavy mineral provenance in the AND-2A drill core, Ross Sea, Antarctica, Global Planet. Change, 82, 38-50, doi:10.1016/j.gloplacha.2011.11.003, 2012.

Henjes-Kunst, F. and Schussler, U.: Metasedimentary units of the Cambro-Ordovician Ross Orogen in northern Victoria Land and Oates Land: implications for their provenance and geotectonic setting from geochemical and Nd-Sr isotope data, Terra Ant. Reports, 10, 105-128, 2003.

https://doi.org/10.5194/gmd-2023-8
Preprint. Discussion started: 17 March 2023

Hergt, J. M., Chappell, B. W., Faure, G. and Mensing, T. M.: The geochemistry of Jurassic dolerites from Portal Peak, Antarctica, Contrib. Mineral. Petr., 102, 298-305, doi:10.1007/BF00373722, 1989.

Hillenbrand, C. D., Baesler, A. and Grobe, H.: The sedimentary record of the last glaciation in the western Bellingshausen Sea (West Antarctica): implications for the interpretation of diamictons in a polar-marine setting, Mar. Geol., 21, 191-204, doi10.1016/j.margeo.2005.01.007, 2005.

Hillenbrand, C. D., Crowhurst, S. J., Williams, M., Hodell, D. A., McCave, I. N., Ehrmann, W., Xuan, C., Piotrowski, A.M., Hernendez-Molina, F.J., Graham, A.G.C., Gorbe, H., Williams, T.J., Horrocks, J.R., Allen, C.S. and Larter, R. D.: New insights from multi-proxy data from the West Antarctic continental rise: Implications for dating and interpreting Late Quaternary palaeoenvironmental records, Quaternary Sci. Rev., 257, 106842, doi: 10.1016/j.quascirev.2021.106842, 2021.

Hillenbrand, C. D. and Ehrmann, W.: Late Neogene to Quaternary environmental changes in the Antarctic Peninsula region: evidence from drift sediments, Global Planet. Change, 45, 165-191, doi:10.1016/j.gloplacha.2004.09.006, 2005.

Hogan, K.A., Larter, R.D., Graham, A.G., Arthern, R., Kirkham, J.D., Totten Minzoni, R., Jordan, T.A., Clark, R., Fitzgerald, V., Wåhlin, A.K. and Anderson, J.B.: Revealing the former bed of Thwaites Glacier using sea-floor bathymetry: implications for warm-water routing and bed controls on ice flow and buttressing, The Cryosphere, 14, 2883-2908, doi:10.5194/tc-14-2883-2020, 2020.

Hopwood, M. J., Carroll, D., Höfer, J., Achterberg, E. P., Meire, L., Le Moigne, F.A.C., Bach, L.T., Eich, C., Sutherland, D.A. and González, H. E.: Highly variable iron content modulates iceberg-ocean fertilisation and potential carbon export, Nat. Commun., 10, 1-10, doi: 10.1038/s41467-019-13231-0, 2019.

Jamieson, S. S., Sugden, D. E. and Hulton, N. R.: The evolution of the subglacial landscape of Antarctica, Earth Planet. Sc. Lett., 293, 1-27, doi:10.1016/j.epsl.2010.02.012, 2010.

Johnson, G. L., Kyle, P. R., Vanney, J. R. and Campsie, J.: Geology of Scott and Balleny Islands, Ross Sea, Antarctica, and morphology of adjacent seafloor. New Zeal. J. Geol. Geop., 25, 427-436, doi:10.1080/00288306.1982.10421508, 1982.

Jordan, T. A., Ferraccioli, F., Armadillo, E. and Bozzo, E.: Crustal architecture of the Wilkes Subglacial Basin in East Antarctica, as revealed from airborne gravity data, Tectonophysics, 585, 196-206, doi:0.1016/j.tecto.2012.06.041, 2013a.

Jordan, T. A., Ferraccioli, F., Ross, N., Corr, H. F., Leat, P. T., Bingham, R. G., Rippin, D.M., le Brocq, A. and Siegert, M. J.: Inland extent of the Weddell Sea Rift imaged by new aerogeophysical data, Tectonophysics, 585, 137-160, doi:10.1016/j.tecto.2012.09.010, 2013b.

Jordan, T. A., Kulessa, B., Thompson, S. and Ferraccioli, F.: Geological Template of the Thwaites Glacier Catchment [Conference Presentation], AGU Fall Meeting, 2020b.

Jordan, T. A., Riley, T. R. and Siddoway, C. S.: The geological history and evolution of West Antarctica, Nat. Rev. Earth & Environment, 1, 117-133, doi:10.1038/s43017-019-0013-6, 2020a.

Kellogg, T. and Kellogg, D.: Antarctic cryogenic sediments: biotic and inorganic facies of ice shelf and marine-based ice sheet environments. Palaeogeogr., Palaeocl., 67, 51-74, doi:10.1016/0031-0182(88)90122-8, 1988.

Kellogg, T., Kellogg, D. and Stuiver, M.: Late Quaternary history of the southwestern Ross Sea: evidence from debris bands on the McMurdo Ice Shelf, Antar. Res. Ser., 50, 25-56, doi: 10.1029/AR050p0025, 1990.

Kipf, A., Hauff, F., Werner, R., Gohl, K., van den Bogaard, P., Hoernle, K., Maicher, D. and Klügel, A.: Seamounts off the West Antarctic margin: A case for non-hotspot driven intraplate volcanism, Gondwana Res., 25, 1660-1679, doi:10.1016/j.gr.2013.06.013, 2014.

Korhonen, F. J., Saito, S., Brown, M., Siddoway, C. S. and Day, J. M. D.: Multiple generations of granite in the Fosdick Mountains, Marie Byrd Land, West Antarctica: implications for polyphase intracrustal differentiation in a continental margin setting, J. Petrol., 51, 627-670, doi:10.1093/petrology/egp093, 2010.

https://doi.org/10.5194/gmd-2023-8
Preprint. Discussion started: 17 March 2023

Lawver, L., Lee, J., Kim, Y. and Davey, F.: Flat-topped mounds in western Ross Sea: Carbonate mounds or subglacial volcanic features?, Geosphere, 8, 645-653, doi:10.1130/GES00766.1, 2012.

LeMasurier, W. E. and Landis, C. A.: Mantle-plume activity recorded by low-relief erosion surfaces in West Antarctica and New Zealand, Geol. Soc. Am. Bull., 108, 1450-1466, doi:10.1130/0016-7606(1996)108<1450:MPARBL>2.3.CO;2, 1996.

LeMasurier, W. E., Thomson, J. W., Baker, P. E., Kyle, P. R., Rowley, P. D., Smellie, J. L. and Verwoerd, W. J.: Volcanoes of the Antarctic plate and Southern Ocean, Antar. Res. Ser., 48, American Geophysical Union, pp. 487, doi:10.1029/AR048, 1990.

Lepp, A.P., Simkins, L.M., Anderson, J.B., Clark, R.W., Wellner, J.S., Hillenbrand, C.D., Smith, J.A., Lehrmann, A.A., Totten, R., Larter, R.D. and Hogan, K.A.: Sedimentary Signatures of Persistent Subglacial Meltwater Drainage From Thwaites Glacier, Antarctica, Front. Earth Sci., 10, 863200, doi:10.3389/feart.2022.863200, 2022.

Licht, K. J. and Hemming, S. R.: Analysis of Antarctic glacigenic sediment provenance through geochemical and petrologic applications, Quaternary Sci. Rev., 164, 1-24, doi:10.1016/j.quascirev.2017.03.009, 2017

Licht, K. J., Hennessy, A. J. and Welke, B. M.: The U-Pb detrital zircon signature of West Antarctic ice stream tills in the Ross embayment, with implications for Last Glacial Maximum ice flow reconstructions, Antarct. Sci. 26, 687–697, doi:10.1017/S0954102014000315, 2014.

Lindow, J., Kamp, P. J., Mukasa, S. B., Kleber, M., Lisker, F., Gohl, K., Kuhn, G. and Spiegel, C.: Exhumation history along the eastern Amundsen Sea coast, West Antarctica, revealed by low-temperature thermochronology, Tectonics, 35, 2239-2257, doi:10.1002/2016TC004236, 2016.

Lipp, A. G., Roberts, G. G., Whittaker, A. C., Gowing, C. J. and Fernandes, V. M.: River sediment geochemistry as a conservative mixture of source regions: Observations and predictions from the Cairngorms, UK, J. Geophys. Res.-Earth, 125, e2020JF005700, doi:10.1029/2020JF005700, 2020.

Lumborg, U.: Modelling the deposition, erosion, and flux of cohesive sediment through Øresund, Journal of Marine Systems, 56, 179-193, doi:10.1016/j.jmarsys.2004.11.003, 2005.

MacAyeal, D. R.: The basal stress distribution of Ice Stream E, Antarctica, inferred by control methods, J. Geophys. Res.-Sol. Ea., 97, 595-603, doi:10.1029/91JB02454, 1992.

Marschalek, J.W., Zurli, L., Talarico, F., van de Flierdt, T., Vermeesch. P., Carter, A., Beny, F., Bout-Roumazeilles, V., Sangiorgi, F., Hemming, S.R, Perez. L.F., Colleoni, F., Prebble, J.G., van Peer, T.E., Perotti, M., Shevenell, A.E., Browne, I., Kulhanek, D.K., Levy, R., Harwood, D., Sullivan, N.B., Meyers, S.R, Griffith, E.M., Hillenbrand, C.-D., Gasson, E., Siegert, M.J., Keisling, B., Licht, K.J., Kuhn, G., Dodd, J.P., Boshuis, C., De Santis, L., McKay, R.M. and the Expedition 374 Science Party: A large West Antarctic Ice Sheet explains early Neogene sea-level amplitude, Nature, 600, 450–455, doi:10.1038/s41586-021-04148-0, 2021.

Marsland, S. J., Bindoff, N. L., Williams, G. D. and Budd, W. F.: Modeling water mass formation in the Mertz Glacier Polynya and Adélie Depression, east Antarctica, J. Geophys. Res.-Oceans, 109, doi:10.1029/2004JC002441, 2004.

Martin, A. P., Cooper, A. F. and Price, R. C.: Petrogenesis of Cenozoic, alkalic volcanic lineages at Mount Morning, West Antarctica and their entrained lithospheric mantle xenoliths: Lithospheric versus asthenospheric mantle sources, Geochim. Cosmochim. Ac., 122, 127-152, doi:10.1016/j.gca.2013.08.025, 2013.

Massom, R. A., Hill, K. L., Lytle, V. I., Worby, A. P., Paget, M. J. and Allison, I.: Effects of regional fast-ice and iceberg distributions on the behaviour of the Mertz Glacier polynya, East Antarctica, Ann. Glaciol., 33, 391-398, doi:10.3189/172756401781818518, 2001.

McCave, I. N.: Deposition from suspension, Encyclopedia of Geology, Elsevier Science Ltd., Amsterdam, pp 759-770, doi:10.1016/B978-0-08-102908-4.10992-0, 2005.

https://doi.org/10.5194/gmd-2023-8
Preprint. Discussion started: 17 March 2023

McCave, I. N.: Size sorting during transport and deposition of fine sediments: sortable silt and flow speed, in: Developments in Sedimentology, 60, edited by: Rebesco, M. and Camerlenghi, A., Elsevier Science Ltd., 121-142, doi:10.1016/S0070-4571(08)10008-5, 2008.

McCave, I. N. and Hall, I. R.: Size sorting in marine muds: Processes, pitfalls, and prospects for paleoflow-speed proxies, Geochem., Geophy., Geosy., 7, doi:10.1029/2006GC001284, 2006.

Mofjeld, H. O.: Depth dependence of bottom stress and quadratic drag coefficient for barotropic pressure-driven currents, J. Phys. Oceanogr., 18, 1658-1669, doi:10.1175/1520-0485(1988)018<1658:DDOBSA>2.0.CO;2, 1988.

Molzahn, M., Reisberg, L. and Wörner, G.: Os, Sr, Nd, Pb, O isotope and trace element data from the Ferrar flood basalts, Antarctica: evidence for an enriched subcontinental lithospheric source, Earth Planet. Sc. Lett., 144, 529-545, doi:10.1016/S0012-821X(96)00178-1, 1996.

Monien, D., Kuhn, G., von Eynatten, H. and Talarico, F. M.: Geochemical provenance analysis of fine-grained sediment revealing Late Miocene to recent Paleo-Environmental changes in the Western Ross Sea, Antarctica, Global Planet. Change, 96, 41-58, doi: 10.1016/j.gloplacha.2010.05.001, 2012.

Morlighem, M., Rignot, E., Binder, T., Blankenship, D., Drews, R., Eagles, G., Eisen, O., Farraccioli, F., Forsburg, R., Fretwell, P., Goel., V., Greenbaum, J.S., Gudmundsson, H., Guo, J., Helm, V., Hofstede, C., Howat, I., Humbert, A., Jokat, W., Karlsson, N.B., Lee, W.S., Matsuoka, K., Millan, R., Mouginot, J., Paden, J., Pattyn, F., Roberts, J., Rosier, S., Ruppel, A., Seroussi, H., Smith, E.C., Steinhage, D., Sun, B., van den Broeke, M.R., van Ommen, T.D., van Wessem, M. and Young, D. A.: Deep glacial troughs and stabilizing ridges unveiled beneath the margins of the Antarctic ice sheet, Nat. Geosci., 13, 132-137, doi:10.1038/s41561-019-0510-8, 2020.

Morlighem, M., Seroussi, H., Larour, E. and Rignot, E.: Inversion of basal friction in Antarctica using exact and incomplete adjoints of a higher-order model, J. Geophys. Res.-Earth, 118, 1746-1753, doi:10.1002/jgrf.20125, 2013.

Mouginot, J., Scheuchl, B. and Rignot. E.: MEaSUREs Antarctic Boundaries for IPY 2007-2009 from Satellite Radar, Version 2, NASA National Snow and Ice Data Center Distributed Active Archive Center, doi:10.5067/AXE4121732AD, 2017.

Mulder, T. : Gravity processes and deposits on continental slope, rise and abyssal plains, in: Developments in Sedimentology, 63, edited by: H. Huneke and T. Mulder, 25-148, Elsevier, doi:10.1016/B978-0-444-53000-4.00002-02011.

Nicholls, K. W., Corr, H. F. J., Makinson, K. and Pudsey, C. J.: Rock debris in an Antarctic ice shelf, Ann. Glaciol., 53, 235-240, doi:10.3189/2012AoG60A014, 2012.

Orejola, N., Passchier, S. and the IODP Expedition 318 Scientists: Sedimentology of lower Pliocene to Upper Pleistocene diamictons from IODP Site U1358, Wilkes Land margin, and implications for East Antarctic ice sheet dynamics, Antarct. Sci., 26, 183-192, doi:10.1017/S0954102013000527, 2014.

Orheim, O., Giles, B., Moholdt, G., Jacka, J. and Bjørdal, A.: The SCAR International Iceberg Database, Norwegian Polar Institute [Data set], doi:10.21334/npolar.2021.e4b9a604, 2021.

Orsi, A. H., Whitworth III, T. and Nowlin Jr, W. D.: On the meridional extent and fronts of the Antarctic Circumpolar Current. Deep-Sea Res. Pt. I, 42, 641-673, doi:10.1016/0967-0637(95)00021-W, 1995

Orsi, A. H. and Wiederwohl, C. L.: A recount of Ross Sea waters. Deep-Sea Res. Pt. II, 56, 778-795, doi: 10.1016/j.dsr2.2008.10.033, 2009.

Pandey, M., Pant, N. C., Biswas, P., Shrivastava, P. K., Joshi, S. and Nagi, N.: Heavy mineral assemblage of marine sediments as an indicator of provenance and east Antarctic ice sheet fluctuations, Geo. Soc. S. P., 461, 95-111, doi:10.1144/SP461.2, 2018.

https://doi.org/10.5194/gmd-2023-8
Preprint. Discussion started: 17 March 2023

Pankhurst, R. J., Millar, I. L., Grunow, A. M. and Storey, B. C.: The pre-Cenozoic magmatic history of the Thurston Island crustal block, West Antarctica, J. Geophys. Res.-Earth, 98, 11835-11849, doi:10.1029/93JB01157, 1993.

Pankhurst, R. J., Storey, B. C. and Millar, U.: Magmatism related to the break-up of Gondwana, edited by: Crame, J. A. and Thomson, J. W, Geological evolution of Antarctica, Volume 1, Cambridge University Press, 573-579, 1991.

Pankhurst, R. J., Weaver, S. D., Bradshaw, J. D., Storey, B. C. and Ireland, T. R.: Geochronology and geochemistry of pre-Jurassic superterranes in Marie Byrd Land, Antarctica, J. Geophys. Res.-Earth, 103, 2529-2547, doi:10.1029/97JB02605, 1998.

Panter, K. S. and Castillo, P.: Petrogenesis and source of lavas from seamounts in the Adare Basin, Western Ross Sea: Implications for the origin of Cenozoic magmatism in Antarctica, in: Antarctica: A Keystone in a Changing World, Online Proceedings of the 10th ISAES X, USGS Open-File Report 2007-1047, Extended Abstract 69, 2007.

Paolo, F. S., Fricker, H. A. and Padman, L.: Volume loss from Antarctic ice shelves is accelerating, Science, 348, 327-331, doi: 10.1126/science.aaa0940, 2015.

Patrick, M. R. and Smellie, J. L.: Synthesis A spaceborne inventory of volcanic activity in Antarctica and southern oceans, 2000–10, Antarct. Sci., 25, 475-500, doi:10.1017/S0954102013000436, 2013.

Paxman, G. J., Jamieson, S. S., Ferraccioli, F., Jordan, T. A., Bentley, M. J., Ross, N., Forsberg, R., Matsuoka, K., Steinhage, D., Eagles, G. and Casal, T. G.: Subglacial Geology and Geomorphology of the Pensacola-Pole Basin, East Antarctica, Geochem., Geophy., Geosy., 20, 2786-2807, doi: 10.1029/2018GC008126, 2019.

Perotti, M., Andreucci, B., Talarico, F., Zattin, M. and Langone, A.: Multianalytical provenance analysis of Eastern Ross Sea LGM till sediments (Antarctica): Petrography, geochronology, and thermochronology detrital data, Geochem., Geophy., Geosy., 18, 2275-2304, doi:10.1002/2016GC006728, 2017.

Pettit, E. C., Whorton, E. N., Waddington, E. D. and Sletten, R. S.: Influence of debris-rich basal ice on flow of a polar glacier, J. Glaciol., 60, 989-1006, doi:10.3189/2014JoG13J161, 2014.

Peucat, J. J., Ménot, R. P., Monnier, O. and Fanning, C. M.: The Terre Adélie basement in the East-Antarctica Shield: geological and isotopic evidence for a major 1.7 Ga thermal event; comparison with the Gawler Craton in South Australia, Precambrian Res., 94, 205-224, doi:10.1016/S0301-9268(98)00119-3, 1999.

Phillips, E. H. Sims, K.W.W., Blichert-Toft, J., Aster, R.C., Gaetani, G.A., Kyle, P.R., Wallace, P.J. and Rasmussen, D.J.: The nature and evolution of mantle upwelling at Ross Island, Antarctica, with implications for the source of HIMU lavas, Earth Planet. Sc. Lett., 498, 38-53, doi:10.1016/j.epsl.2018.05.049, 2018.

Pierce, E. L., Williams, T., Van De Flierdt, T., Hemming, S. R., Goldstein, S. L. and Brachfeld, S. A.: Characterizing the sediment provenance of East Antarctica's weak underbelly: The Aurora and Wilkes sub-glacial basins, Paleoceanography, 26, PA4217, doi.org/10.1029/2011PA002127, 2011.

Pollard, D. and DeConto, R. M.: Description of a hybrid ice sheet-shelf model, and application to Antarctica, Geosci. Model Dev., 5, 1273-1295, doi:10.5194/gmd-5-1273-2012, 2012.

Pollard, D. and DeConto, R. M.: Continuous simulations over the last 40 million years with a coupled Antarctic ice sheet-sediment model, Palaeogeogr. Palaeocl., 537, 109374, doi: 10.1016/j.palaeo.2019.109374, 2019.

Prestvik, T. and Duncan, R. A.: The geology and age of Peter I Øy, Antarctica, Polar Res., 9, 89-98, doi:10.3402/polar.v9i1.6781, 1991.

Rackow, T., Wesche, C., Timmermann, R., Hellmer, H. H., Juricke, S. and Jung, T.: A simulation of small to giant Antarctic iceberg evolution: Differential impact on climatology estimates, J. Geophys. Res.-Oceans, 122, 3170-3190, doi: 10.1002/2016JC012513, 2017.

Rignot, E., Jacobs, S., Mouginot, J. and Scheuchl, B.: Ice-shelf melting around Antarctica, Science, 341, 266-270, doi:10.1126/science.1235798, 2013.

https://doi.org/10.5194/gmd-2023-8
Preprint. Discussion started: 17 March 2023

Rilling, S., Mukasa, S., Wilson, T., Lawver, L. and Hall, C.: New determinations of 40Ar/39Ar isotopic ages and flow volumes for Cenozoic volcanism in the Terror Rift, Ross Sea, Antarctica, J. Geophys. Res.-Earth, 114, doi: 10.1029/2009JB006303, 2009.

Robinson, S., Ivanovic, R., van de Flierdt, T., Blanchet, C.L., Tachikawa, K., Martin, E.E., Cook, C.P., Williams, T., Gregoire, L., Plancherel, Y. and Jeandel, C.: Global continental and marine detrital εNd: An updated compilation for use in understanding marine Nd cycling, Chem. Geol., 567, 120119, doi:10.1016/j.chemgeo.2021.120119, 2021.

Rocchi, S., Di Vincenzo, G., Ghezzo, C. and Nardini, I.: Granite-lamprophyre connection in the latest stages of the early Paleozoic Ross Orogeny (Victoria Land, Antarctica), Geol. Soc. Am. Bull., 121, 801-819, doi:10.1130/B26342.1, 2009.

Rocchi, S., Tonarini, S., Armienti, P., Innocenti, F. and Manetti, P.: Geochemical and isotopic structure of the early Palaeozoic active margin of Gondwana in northern Victoria Land, Antarctica, Tectonophysics, 284, 261-281, doi:10.1016/S0040-1951(97)00178-9, 1998.

Rodrigues, S., Hernández-Molina, F. J., Hillenbrand, C. D., Lucchi, R. G., Rodríguez-Tovar, F. J., Rebesco, M. and Larter, R. D.: Recognizing key sedimentary facies in mixed depositional systems: the case of the Pacific margin of the Antarctic Peninsula, Sedimentology, 69, 1953-1991, doi: 10.1111/sed.12978, 2022b.

Rodrigues, S., Hernández-Molina, F. J., Larter, R. D., Rebesco, M., Hillenbrand, C. D., Lucchi, R. G., and Rodríguez-Tovar, F. J.: Sedimentary model for mixed depositional systems along the Pacific margin of the Antarctic Peninsula: Decoding the interplay of deep-water processes, Mar. Geol., 445, 106754, doi:10.1016/j.margeo.2022.106754, 2022a.

Russell-Head, D. S.: The melting of free-drifting icebergs, Ann. Glaciol., 1, 119-122, doi:10.3189/S0260305500017092, 1980.

Sandroni, S. and Talarico, F. M.: The record of Miocene climatic events in AND-2A drill core (Antarctica): Insights from provenance analyses of basement clasts, Global Planet Change, 75, 31-46, doi:10.1016/j.gloplacha.2010.10.002, 2011.

Schroeder, D. M., Blankenship, D. D., Young, D. A. and Quartini, E.: Evidence for elevated and spatially variable geothermal flux beneath the West Antarctic Ice Sheet, P. Natl. Acad. Sci. USA, 111, 9070-9072, doi:10.1073/pnas.1405184111, 2014.

Shao, H., He, J., Wu, L. and Wei, L.: Elemental and Sr–Nd isotopic compositions of surface clay-size sediments in the front end of major ice shelves around Antarctica and indications for provenance, Deep-Sea Res. Pt. II, 195, 105011, doi: 10.1016/j.dsr2.2021.105011, 2022.

Shaw, T. J., Raiswell, R., Hexel, C. R., Vu, H. P., Moore, W. S., Dudgeon, R. and Smith Jr, K. L.: Input, composition, and potential impact of terrigenous material from free-drifting icebergs in the Weddell Sea, Deep-Sea Res. Pt. II, 58, 1376-1383, doi:10.1016/j.dsr2.2010.11.012, 2011.

Shi, B., Wang, Y. P., Yang, Y., Li, M., Li, P., Ni, W. and Gao, J.: Determination of critical shear stresses for erosion and deposition based on in situ measurements of currents and waves over an intertidal mudflat, J. Coastal Res., 31, 1344-1356, doi:10.2112/JCOASTRES-D-14-00239.1, 2015.

Simões Pereira, P., van de Flierdt, T., Hemming, S. R., Frederichs, T., Hammond, S. J., Brachfeld, S., Doherty, C., Kuhn, G., Smith, J.A., Klages, J.P. and Hillenbrand, C. D.: The geochemical and mineralogical fingerprint of West Antarctica's weak underbelly: Pine Island and Thwaites glaciers, Chem. Geol., 550, 119649, doi:10.1016/j.chemgeo.2020.119649, 2020.

Simões Pereira, P., van de Flierdt, T., Hemming, S. R., Hammond, S. J., Kuhn, G., Brachfeld, S., Doherty, C. and Hillenbrand, C. D.: Geochemical fingerprints of glacially eroded bedrock from West Antarctica: Detrital thermochronology, radiogenic isotope systematics and trace element geochemistry in Late Holocene glacial-marine sediments, Earth-Sci. Rev., 182, 204-232, doi:10.1016/j.earscirev.2018.04.011, 2018.

https://doi.org/10.5194/gmd-2023-8
Preprint. Discussion started: 17 March 2023

Smith, J. A., Graham, A. G., Post, A. L., Hillenbrand, C. D., Bart, P. J. and Powell, R. D.: The marine geological imprint of Antarctic ice shelves, Nat. Commun., 10, 1-16, doi:10.1038/s41467-019-13496-5, 2019.

Smith, J. A., Hillenbrand, C. D., Larter, R. D., Graham, A. G. and Kuhn, G.: The sediment infill of subglacial meltwater channels on the West Antarctic continental shelf, Quaternary Res., 71, 190-200, doi:10.1016/j.yqres.2008.11.005, 2009.

Storey, B. C., Pankhurst, R. J. and Johnson, A. C.: The Grenville Province within Antarctica: a test of the SWEAT hypothesis, J. Geol. Soc. London, 151, 1-4, doi:10.1144/gsjgs.151.1.0001, 1994.

Stow, D.A.V.: Deep sea processes of sediment transport and deposition, Sediment Transport and Depositional Processes, edited by Pye K., Blackwell Scientific Publications, Oxford, 257-291, 1994.

Struve, T., van de Flierdt, T., Burke, A., Robinson, L. F., Hammond, S. J., Crocket, K. C., Bradtmiller, L.I., Auro, M.E., Mohanmed, K.J. and White, N. J.: Neodymium isotopes and concentrations in aragonitic scleractinian cold-water coral skeletons-Modern calibration and evaluation of palaeo-applications, Chem. Geol., 453, 146-168, doi:10.1016/j.chemgeo.2017.01.022, 2017.

Stuart, K. M. and Long, D. G.: Tracking large tabular icebergs using the SeaWinds Ku-band microwave scatterometer, Deep-Sea Res. Pt. II, 58, 1285-1300, doi:10.1016/j.dsr2.2010.11.004, 2011.

Studinger, M., Bell, R. E., Fitzgerald, P. G. and Buck, W. R.: Crustal architecture of the Transantarctic Mountains between the Scott and Reedy Glacier region and South Pole from aerogeophysical data, Earth Planet. Sc. Lett., 250, 182-199, doi:10.1016/j.epsl.2006.07.035, 2006.

Talarico, F., Borsi, L. and Lombardo, B.: Relict granulites in the Ross Orogen of northern Victoria Land (Antarctica), II. Geochemistry and palaeo-tectonic implications, Precambrian Res., 75, 157-174, doi:10.1016/0301-9268(95)80004-2, 1995.

Tonarini, S. and Rocchi, S.: Geochronology of Cambro-Ordovician intrusives in Victoria Land: A review, Terra Ant. Reports, 1, 46-50, 1994.

Tournadre, J., Bouhier, N., Girard-Ardhuin, F.and Rémy, F.: Antarctic icebergs distributions 1992–2014, J. Geophys. Res.-Oceans, 121, 327-349, doi:10.1002/2015JC011178, 2016.

Tucholke, B. E.: Sedimentation processes and acoustic stratigraphy in the Bellingshausen Basin, Mar. Geol., 25, 209-230, doi:10.1016/0025-3227(77)90053-6, 1977.

Umlauf, L. and Arneborg, L.: Dynamics of rotating shallow gravity currents passing through a channel. Part I: Observation of transverse structure, J. Phys. Oceanogr., 39, 2385-2401, doi:10.1175/2009JPO4159.1, 2009.

van de Flierdt, T., Goldstein, S. L., Hemming, S. R., Roy, M., Frank, M. and Halliday, A. N.: Global neodymium–hafnium isotope systematics—revisited, Earth Planet. Sc. Lett., 259, 432-441, doi: 10.1016/j.epsl.2007.05.003, 2007.

van Wyck de Vries, M., Bingham, R. G. and Hein, A. S.: A new volcanic province: an inventory of subglacial volcanoes in West Antarctica, Geo. Soc. S. P., 461, 231-248, doi:10.1144/SP461.7, 2018.

Wagner, T. J., Dell, R. W. and Eisenman, I.: An analytical model of iceberg drift. J. Phys. Oceanogr., 47, 1605-1616, doi:10.1175/JPO-D-16-0262.1, 2017.

Walter, H. J., Hegner, E., Diekmann, B. and Kuhn, G.: Provenance and transport of terrigenous sediment in the South Atlantic Ocean and their relations to glacial and interglacial cycles: Nd and Sr isotopic evidence, Geochim. Cosmochim. Ac., 64, 3813-3827, doi:10.1016/S0016-7037(00)00476-2, 2000.

Wang, X., Holland, D. M. and Gudmundsson, G. H.: Accurate coastal DEM generation by merging ASTER GDEM and ICESat/GLAS data over Mertz Glacier, Antarctica, Proc Spie, 206, 218-230, doi:10.1016/j.rse.2017.12.041, 2018.

Wareham, C. D., Stump, E., Storey, B. C., Millar, I. L. & Riley, T. R.: Petrogenesis of the Cambrian Liv Group. A bimodal volcanic rock suite from the Ross orogen, Transantarctic Mountains, Geol. Soc. Am. Bull., 113, 360–372, doi:10.1130/0016-7606(2001)113<0360:POTCLG>2.0.CO;2, 2001.

https://doi.org/10.5194/gmd-2023-8
Preprint. Discussion started: 17 March 2023

Weaver, S. D., Adams, C. J., Pankhurst, R. J. and Gibson, I. L.: Granites of Edward VII Peninsula, Marie Byrd Land: anorogenic magmatism related to Antarctic-New Zealand rifting, T. RSE Earth, 83, 281-290, doi:10.1017/S0263593300007963, 1992.

Weis, D., Kieffer, B., Maerschalk, C., Barling, J., De Jong, J., Williams, G.A., Hanano, D., Pretorius, W., Mattielli, N., Scoates, J.S. and Goolaerts, A.: High-precision isotopic characterization of USGS reference materials by TIMS and MC-ICP-MS. Geochem., Geophy., Geosy., 7, doi: 10.1029/2006GC001283, 2006.

Williams, T., Hemming, S. R., Licht, K., Agrios, L., Brachfeld, S. A., van de Flierdt, T., Hillenbrand, C.D., Ehrmann, W.U., Zhai, X., Cai, Y. and Corley, A.D. and Kuhn, G.: Insights into the Geographic Sequence of Deglaciation in the Weddell Sea Embayment by Provenance of Ice-Rafted Debris, AGU Fall Meeting, New Orleans, 11-15th December 2017, C21E-1168, 2017.

Wilson, D. J., Bertram, R. A., Needham, E. F., van de Flierdt, T., Welsh, K. J., McKay, R. M., Mazumder, A., Riesselman, C.R., Jimnez-Espejo, F.J. and Escutia, C.: Ice loss from the East Antarctic Ice Sheet during late Pleistocene interglacials, Nature, 561, 383-386, doi:10.1038/s41586-018-0501-8, 2018.

Yakymchuk, C., Brown, C. R., Brown, M., Siddoway, C. S., Fanning, C. M. and Korhonen, F. J.: Paleozoic evolution of western Marie Byrd Land, Antarctica, Geol. Soc. Am. Bull., 127, 1464-1484, doi:10.1130/B31136.1, 2015.

Zuo, H., Balmaseda, M. A., Tietsche, S., Mogensen, K. and Mayer, M.: The ECMWF operational ensemble reanalysis–analysis system for ocean and sea ice: a description of the system and assessment, Ocean Sci., 15, 779-808, doi:10.5194/os-15-779-2019, 2019.